Analytic modal solution to light propagation through layer-by-layer metallic photonic crystals

Zhi-Yuan Li and Kai-Ming Ho
Ames Laboratory and Department of Physics and Astronomy, Iowa State University, Ames, Iowa 50011
(Received 3 October 2002; revised manuscript received 17 December 2002; published 14 April 2003)

An analytic modal expansion method combined with a transfer-matrix technique is developed to investigate the reflection, transmission, and absorption spectra of three-dimensional layer-by-layer metallic photonic crystals working in a regime from microwave to infrared wavelengths. The eigenmodes for electromagnetic fields within each layer of the crystal are solved analytically by matching boundary conditions. The eigenmodes are then projected onto a plane wave basis, so that the scattering problem for a multilayer structure can be cast into the framework of transfer-matrix method. In addition, the structural symmetry between different layers of the crystal is fully exploited to connect the transfer matrix for different layers and significantly reduce the computation effort on the light scattering problem. Fast convergence of numerical result has been obtained and excellent agreement of theoretical results with experimental measurements has been achieved, indicating the effectiveness and efficiency of the developed analytical modal expansion method.

DOI: 10.1103/PhysRevB.67.165104 PACS number(s): 42.70.Qs, 41.20.Jb, 78.70.Gq

I. INTRODUCTION

Photonic crystals, a class of material giving rise to a range of frequency called a photonic band gap (PBG) within which electromagnetic (EM) waves cannot propagate along any direction, provide a powerful way to manipulate and control the flow of photons in much the same way as conventional semiconductors do to electrons.[1,2] In recent years metallic photonic crystals have attracted much attention because of the large PBG present[3–10] and potential applications in microwave regimes such as filters. Most experimental works were done in the microwave regime, and metal in this regime can be assumed as a perfect reflector. Very recently, a three-dimensional (3D) metallic photonic crystal working in the midinfrared (IR) wavelength was successfully achieved by means of state-of-the-art lithographic techniques[10] under a layer-by-layer stacking scheme.[11–14] Even in this long wavelength regime, the absorptive and dispersive properties of metal has already become apparent.[10] It is the aim of this paper to present a simple, efficient, and rigorous theoretical model to investigate the propagation behavior of EM waves through this important class of metallic photonic crystal structures in a regime from microwave to infrared wavelengths.

For a metallic photonic crystal structure, the usual plane-wave expansion method[15,16] becomes ineffective. Other theoretical approaches have been employed as an alternative, such as the finite-difference time-domain method[6] and the multiscattering method[9,17,18] based on the Korringa-Kohn-Rostoker theory (which is limited to photonic crystals made of particles inscribed to nonoverlapping spheres or cylinders). The propagation of EM waves through a 3D photonic crystal slab with a finite thickness can be cast into the framework of scattering of EM waves by a 2D grating. EM approaches such as the coupled-wave method[19–21] in the Fourier space and the real-space transfer-matrix method[22,23] have been developed to study the transmission and reflection spectra of 1D and 2D gratings. However, severe convergence difficulty is found in both methods for a highly conducting 2D grating due to a skin depth two orders of magnitude smaller than the incident wavelength. A large number of plane waves in the coupled-wave method or very fine mesh of grid point in the real-space transfer-matrix method is required to account for this small skin depth effect. To attack the theoretical challenge for a 2D metallic layer-by-layer grating scaled from mid-IR to microwave wavelengths, we have developed an EM approach which combines a series of techniques ranging from analytic modal expansion method, to the transfer-matrix method, and to the application of structural symmetry. A fast-convergent solution of the spectra has been obtained and excellent agreement with experimental measurements has been achieved.

Before we move into the very detailed discussions on how the developed method is working for a metallic photonic crystal slab, we will first present here a brief description of the general idea. Let us first take a close look at a layer-by-layer photonic crystal. A 3D schematic picture of the crystal structure is shown in Fig. 1(a). The top-view picture of this photonic crystal from the (001) direction is also displayed in Fig. 1(b). The metallic photonic crystal is formed by stacking rectangular metallic rods layer by layer consecutively along the (001) direction. Rods in each layer are arrayed into a one-dimensional periodic structure—a lamellar grating with a pitch of d. Rods in one layer are perpendicular to those in the adjacent layers, while rods in one layer are shifted by $d/2$ with respect to those in the second-nearest neighboring layers. The primitive unit cell of the photonic crystal is arrayed into a face-centered tetragonal (fct) lattice. In Figs. 1(a) and 1(b), we have assumed that rods in the first layer are along the y axis, and rods in the second layer are along the x axis direction, and so on. The rods each has a width of w, a thickness of h, and form a square lattice with a lattice spacing of d in the (001) plane. Every four layers of rods comprise a repeating unit cell along the (001) direction of the crystal.

The layer-by-layer photonic crystal is an interconnected topological network with a complex surface geometry, therefore, the usual method to match boundary conditions at every air-metal wall of the whole crystal is quite troublesome. To overcome this difficulty, several tricks have been used in our

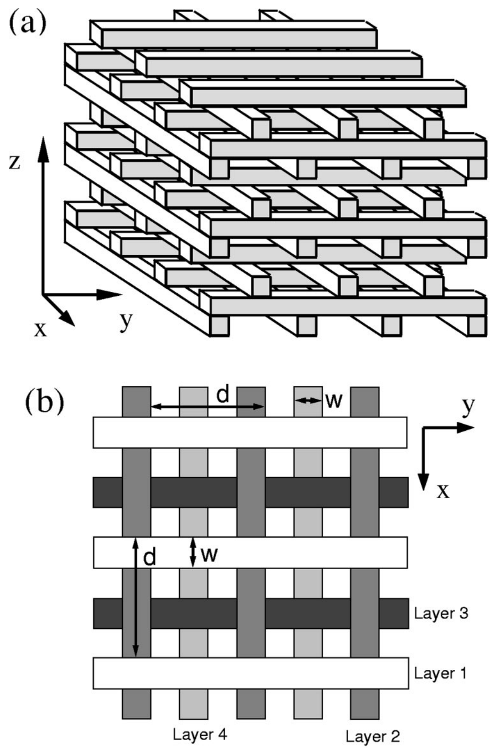

FIG. 1. (a) Schematical configuration of a 3D layer-by-layer photonic crystal composed of rectangular metallic rods in air. (b) Top-view picture of (a) from the (001) direction, the stacking direction of the crystal layers.

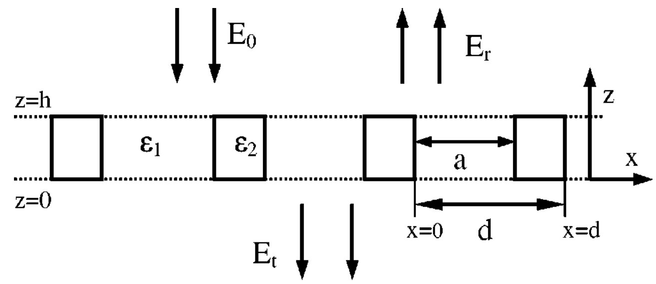

FIG. 2. Schematical configuration of a plane EM wave scattered by a 1D metallic lamellar grating. The grating has a pitch of d, thickness of h, and an air-domain size of a. The dielectric constant for the air and metal domain is ϵ_1 and ϵ_2, respectively. E_0, E_r, and E_t are the incident, reflection, and transmission waves, respectively.

method developed in this work. First, as one has noticed above, each layer of the photonic crystal is just a 1D lamellar grating. This specific configuration allows us to use analytical solution of EM modes inside each 1D lamellar grating. Second, for a multilayer photonic crystal slab, we can treat the wave scattering by each single layer separately, and then combine all layers using the transfer-matrix technique. This enables us to examine the scattering problem of a multilayer structure in a systematical manner, and brings great flexibility. Third, one can further notice that there are several structural symmetries between different layers of the crystal. If fully considered and exploited, these symmetries can significantly reduce the scattering problem for all different layers into that for only one single layer. Therefore, virtually only a 1D scattering problem needs to be attacked. This is another big saving of theoretical and numerical efforts from those for a general 2D scattering problem.

Following the general ideas outlined above, we arrange this paper as follows. In Sec. II we will deal with general scattering problem for a 1D perfect-conducting lamellar grating under off-plane conical wave incidence. Modal expansion and moment techniques will be used. This will lay down a basis for our later discussions on general 2D scattering problems. In Sec. III we will move forward to consider scattering by a 2D layer-by-layer photonic crystal grating made up of perfect-conducting metallic materials. The transfer-matrix method will be introduced in combination with the modal expansion techniques. In addition, application of structural symmetries to the transfer-matrix method will be discussed. In Sec. IV, we will follow the similar theoretical framework to solve the scattering problem of a metallic layer-by-layer photonic crystal grating working in the mid-IR wavelengths, where the metallic material is highly conducting. In Sec. V, we will apply the developed theoretical tools to examine two experiments on metallic layer-by-layer photonic crystals in order to demonstrate the power and efficiency of the developed method. One experiment is concerned with the microwave regime, the other is working in the mid-IR regime. Finally in Sec. VI, we will present some concluding remarks.

II. EM WAVES SCATTERING BY 1D PERFECT-CONDUCTING LAMELLAR GRATINGS

As we have noticed in the Introduction, each layer of the considered layer-by-layer photonic crystal is a 1D lamellar grating along the stacking direction. This reminds us that in our first step we should have a clear understanding on how to solve this 1D scattering problem. To correspond well to the scattering problem of 2D grating, we must consider general incidence condition (so-called off-plane conical incidence) for the 1D grating, namely, arbitrary incident angles and polarizations. However, it is helpful to first start from the simplest case of in-plane incidence, where the incident wave vector lies in the plane perpendicular to the grating axis (direction where the dielectric function keeps constant). In this situation we have two eigenmodes for the scattering problem, the TE and TM modes, in which either the electric or the magnetic field is parallel to the grating axis. This problem has been investigated extensively in literatures,[24–27] and useful ideas and techniques have been developed, therefore, we will not repeat it here. Interested readers can refer to original literatures. In the following, we will extend the ideas and techniques to general off-plane conical incidence situations.

The schematic configuration of the scattering problem is depicted in Fig. 2, where the 1D perfect-conducting grating is supposed to extend along the y-axis direction, and repeat its unit cell along the x-axis direction every distance of d. The air-metal interface is located at $x=0$ and $x=a$, respectively. In the situation of general off-plane conical incidence, a plane wave is incident on the 1D grating from up to down along the $-z$ direction with a wave vector $\mathbf{k}_0$

$=(k_{0x},k_{0y},k_{0z})=k_0(\sin\theta\cos\phi,\sin\theta\sin\phi,\cos\theta)$, where $k_0=(\omega/c)$ is the wave number, ω is the angular frequency, c is the light speed in vacuum. θ and ϕ are the incident polar and azimuthal angles, with $\pi/2\leqslant\theta<\pi$, and $0\leqslant\phi<2\pi$. In the conical incidence, the TE and TM modes are no longer the eigenmodes of a 1D grating, instead, they are coupled with each other. Since the grating is homogeneous along the y-axis direction, the y-axis wave vector component is a constant k_{0y} in the process of the wave scattering.

The **E** and **H** fields in the incidence and transmission regions are both composed of three components. We first consider EM fields in the incidence region $\mathbf{E}_r$ and $\mathbf{H}_r$. In the plane-wave basis, the tangential components of $\mathbf{E}_r$ are written in general forms as

$$E_x(\mathbf{r})=\sum_{i=-\infty}^{\infty} E_{ij,x}(z)e^{ik_{ix}x+ik_{jy}y}=\sum_{i=-\infty}^{\infty}[E_{ij,x}^{+}(z)+E_{ij,x}^{-}(z)]e^{ik_{ix}x+ik_{jy}y}, \quad (2.1a)$$

$$E_y(\mathbf{r})=\sum_{i=-\infty}^{\infty} E_{ij,y}(z)e^{ik_{ix}x+ik_{jy}y}=\sum_{i=-\infty}^{\infty}[E_{ij,y}^{+}(z)+E_{ij,y}^{-}(z)]e^{ik_{ix}x+ik_{jy}y}. \quad (2.1b)$$

Here $k_{ix}=k_{0x}+i2\pi/d$, $k_{jy}=k_{0y}$, $E_{ij,x(y)}^{+}(z)=E_{ij,x(y)}^{+}e^{i\beta_{ij}(z-h)}$, $E_{ij,x(y)}^{-}(z)=E_{ij,x(y)}^{-}e^{-i\beta_{ij}(z-h)}$, where $\beta_{ij}=-(k_0^2-k_{ix}^2-k_{jy}^2)^{1/2}$ for $k_0^2-k_{ix}^2-k_{jy}^2\geqslant0$, and $\beta_{ij}=-i(k_{ix}^2+k_{jy}^2-k_0^2)^{1/2}$ for $k_0^2-k_{ix}^2-k_{jy}^2<0$. The definition of β_{ij} are in consistence with the fact that the incident wave is propagating along the $-z$ direction.

The z component $E_z(\mathbf{r})$ can be obtained from $\nabla\cdot\mathbf{E}(\mathbf{r})=0$. The magnetic field can be derived from $\mathbf{H}=(1/ik_0)\nabla\times\mathbf{E}$, and the tangential components are written as

$$H_x(\mathbf{r})=\sum_{i=-\infty}^{\infty} H_{ij,x}(z)e^{ik_{ix}x+ik_{jy}y}\sum_{i=-\infty}^{\infty}[H_{ij,x}^{+}(z)+H_{ij,x}^{-}(z)]e^{ik_{ix}x+ik_{jy}y}, \quad (2.2a)$$

$$H_y(\mathbf{r})=\sum_{i=-\infty}^{\infty} H_{ij,y}(z)e^{ik_{ix}x+ik_{jy}y}=\sum_{i=-\infty}^{\infty}[H_{ij,y}^{+}(z)+H_{ij,y}^{-}(z)]e^{ik_{ix}x+ik_{jy}y}, \quad (2.2b)$$

where $H_{ij,x(y)}^{+}(z)=H_{ij,x(y)}^{+}e^{i\beta_{ij}(z-h)}$, $H_{ij,x(y)}^{-}(z)=H_{ij,x(y)}^{-}e^{-i\beta_{ij}(z-h)}$. For each wave vector we have the following relation between the **H** and **E** fields: $(H_{ij,x}^{+},H_{ij,y}^{+})^T=T_{0,ij}(E_{ij,x}^{+},E_{ij,y}^{+})^T$ and $(H_{ij,x}^{-},H_{ij,y}^{-})^T=-T_{0,ij}(E_{ij,x}^{-},E_{ij,y}^{-})^T$, where the superscript "T" denotes matrix transposition. The 2×2 matrix $T_{0,ij}$ has matrix elements $T_{0,ij}^{11}=-k_{ix}k_{jy}/(k_0\beta_{ij})$, $T_{0,ij}^{12}=(k_{ix}^2-k_0^2)/(k_0\beta_{ij})$, $T_{0,ij}^{21}=(k_0^2-k_{jy}^2)/(k_0\beta_{ij})$, and $T_{0,ij}^{22}=k_{ix}k_{jy}/(k_0\beta_{ij})$. It can be seen that $E^{+}(H^{+})$ and $E^{-}(H^{-})$ correspond to the incident and reflected waves, respectively.

The EM fields in the transmission region $\mathbf{E}_t$ and $\mathbf{H}_t$ have the same general form of expansion

$$E_x(\mathbf{r})=\sum_{i=-\infty}^{\infty} U_{ij,x}(z)e^{ik_{ix}x+ik_{jy}y}=\sum_{i=-\infty}^{\infty}[U_{ij,x}^{+}(z)+U_{ij,x}^{-}(z)]e^{ik_{ix}x+ik_{jy}y}, \quad (2.3a)$$

$$E_y(\mathbf{r})=\sum_{i=-\infty}^{\infty} U_{ij,y}(z)e^{ik_{ix}x+ik_{jy}y}=\sum_{i=-\infty}^{\infty}[U_{ij,y}^{+}(z)+U_{ij,y}^{-}(z)]e^{ik_{ix}x+ik_{jy}y}. \quad (2.3b)$$

$$H_x(\mathbf{r})=\sum_{i=-\infty}^{\infty} V_{ij,x}(z)e^{ik_{ix}x+ik_{jy}y}=\sum_{i=-\infty}^{\infty}[V_{ij,x}^{+}(z)+V_{ij,x}^{-}(z)]e^{ik_{ix}x+ik_{jy}y}, \quad (2.4a)$$

$$H_y(\mathbf{r})=\sum_{i=-\infty}^{\infty} V_{ij,y}(z)e^{ik_{ix}x+ik_{jy}y}=\sum_{i=-\infty}^{\infty}[V_{ij,y}^{+}(z)+V_{ij,y}^{-}(z)]e^{ik_{ix}x+ik_{jy}y}, \quad (2.4b)$$

where $U_{ij,x(y)}^{+}(z)=U_{ij,x(y)}^{+}e^{i\beta_{ij}z}$, $U_{ij,x(y)}^{-}(z)=U_{ij,x(y)}^{-}e^{-i\beta_{ij}z}$. $V_{ij,x(y)}^{+}$ and $V_{ij,x(y)}^{-}$ are also connected to $U_{ij,x(y)}^{+}$ and $U_{ij,x(y)}^{-}$ through the 2×2 matrix $T_{0,ij}$. Obviously $U^{+}(V^{+})$ and $U^{-}(V^{-})$ correspond to forward and backward propagating waves in the transmission region, respectively. Temporarily, we assume that both waves coexist in the transmission region. In reality, $U^{-}(V^{-})$ should vanish, since only transmitted waves exist in this region for our 1D lamellar grating. But we will see in later sections that the introduction of $U^{-}(V^{-})$ into a single-layer 1D grating will bring us great convenience and flexibility to the scattering problem of a general multilayer 2D grating, because they are one of the central elements in the transfer-matrix method.

As noted above, the y component of the wave vector is a constant during the process of EM waves scattering by the 1D grating, therefore, the EM fields $\mathbf{E}_m$ and $\mathbf{H}_m$ inside the grating domain can be written as

$$E_y(\mathbf{r})=\sum_{m=1}^{\infty}(A_m^j\cos\mu_m z+B_m^j\sin\mu_m z)X_m(x)e^{ik_{jy}y}, \quad (2.5)$$

$$E_x(\mathbf{r})=\sum_{m=0}^{\infty}(E_m^j\cos\mu_m z+F_m^j\sin\mu_m z)Y_m(x)e^{ik_{jy}y}, \quad (2.6)$$

$$E_z(\mathbf{r})=\sum_{m=1}^{\infty}[\mu_m^{-1}(ik_{jy}B_m^j-F_m^j s_m)\cos\mu_m z+\mu_m^{-1}(-ik_{jy}A_m^j+E_m^j s_m)\sin\mu_m z]X_m(x)e^{ik_{jy}y}, \tag{2.7}$$

where $s_m=m\pi/a$, a being the width of the air domain, $X_m(x)=(2/a)^{1/2}\sin(s_m x)$, $Y_m(x)=(2/a)^{1/2}\cos(s_m x)$ for $m>0$, and $Y_0(x)=(1/a)^{1/2}$. μ_m is defined as $\mu_m=(k_0^2-s_m^2-k_{jy}^2)^{1/2}$ if $s_m^2+k_{jy}^2\leqslant k_0^2$, and $\mu_m=i(s_m^2+k_{jy}^2-k_0^2)^{1/2}$ if $s_m^2+k_{jy}^2>k_0^2$. It can be shown that each expansion term in Eqs. (2.5)–(2.7) is a solution to Maxwell's equations in the rectangular air slit satisfying the boundary conditions that the tangential components $E_y=0$ and $E_z=0$ at both $x=0$ and $x=a$. From Maxwell's equation $ik_0\mathbf{H}=\nabla\times\mathbf{E}$, we can derive the tangential $\mathbf{H}_m$ components as

$$\begin{aligned}ik_0H_x(\mathbf{r})&=\frac{\partial}{\partial y}E_z-\frac{\partial}{\partial z}E_y\\&=\sum_{m=1}^{\infty}(k_{jy}^2\mu_m^{-1}+\mu_m)\sin\mu_m zA_m^j-(k_{jy}^2\mu_m^{-1}+\mu_m)\\&\quad\times\cos\mu_m zB_m^j+(ik_{jy}\mu_m^{-1}s_m)\sin\mu_m zE_m^j\\&\quad-(ik_{jy}\mu_m^{-1}s_m)\cos\mu_m zF_m^j,\end{aligned} \tag{2.8}$$

$$\begin{aligned}ik_0H_y(\mathbf{r})&=\frac{\partial}{\partial z}E_x-\frac{\partial}{\partial z}E_z\\&=\sum_{m=1}^{\infty}[(ik_{jy}\mu_m^{-1}s_m)\sin\mu_m zA_m^j\\&\quad-(ik_{jy}\mu_m^{-1}s_m)\cos\mu_m zB_m^j\\&\quad-(s_m^2\mu_m^{-1}+\mu_m)\sin\mu_m zE_m^j\\&\quad+(s_m^2\mu_m^{-1}+\mu_m)\cos\mu_m zB_m^j]Y_m(x)e^{ik_{jy}y}\\&\quad+(-\mu_0\sin\mu_0 zE_0^j+\mu_0\cos\mu_0 zF_0^j)Y_0(x)e^{ik_{jy}y}.\end{aligned} \tag{2.9}$$

Now that we have finished the expansion of EM fields in the incidence, grating, and transmission regions, we can go straightforward to find out the unknown field expansion coefficients in the three regions through match of boundary conditions at $z=h$ and $z=0$. From this we have

$$\mathbf{E}_r^{\tan}(z=h)=\mathbf{E}_m^{\tan}(z=h),\quad 0<x<d, \tag{2.10a}$$

$$\mathbf{H}_r^{\tan}(z=h)=\mathbf{H}_m^{\tan}(z=h),\quad 0<x<a, \tag{2.10b}$$

$$\mathbf{E}_t^{\tan}(z=0)=\mathbf{E}_m^{\tan}(z=0),\quad 0<x<d, \tag{2.10c}$$

$$\mathbf{H}_r^{\tan}(z=0)=\mathbf{H}_m^{\tan}(z=0),\quad 0<x<a, \tag{2.10d}$$

where the superscript ''tan'' means the tangential components of fields. Using the technique of moments at $z=h$ and $z=0$ for the electric field, we have projected both hand sides of Eqs. (2.10a) and (2.10c) onto the basis of plane-wave functions. From this we arrive at the following matrix equation after truncation over the infinite linear equations:

$$dZ_0^j=P_1Z_m^j. \tag{2.11}$$

Z_0^j and Z_m^j are column vectors composed of the field expansion coefficients, where the superscript ''j'' refers to the k_{jy} component of the incident wave vector. They are defined by

$$Z_0^j=[E_{ij,x}(h),E_{ij,y}(h),U_{ij,x}(0),U_{ij,y}(0)]^T,$$

$$Z_m^j=(A_m^j,B_m^j,E_0^j,E_m^j,F_0^j,F_m^j)^T,$$

where $E_{ij,x(y)}(h)=[E_{-Nj,x(y)}(h),\dots,E_{0j,x(y)}(h),\dots,E_{Nj,x(y)}(h)]$, $A_m^j=(A_1^j,A_2^j,\dots,A_{M-1}^j)$, etc. The corresponding dimension is $4N_0$ and $4M-2$, where $N_0=2N+1$ and M is the plane wave and modal numbers in the incidence and grating regions. The $(4N_0)\times(4M-2)$ dimensioned matrix P_1 is

$$P_1=\begin{pmatrix}0&0&\cos(\mu_0h)J_{i0}^*&\cos(\mu_mh)J_{im}&\sin(\mu_0h)J_{i0}^*&\sin(\mu_mh)J_{im}\\\cos(\mu_mh)I_{im}^*&\sin(\mu_mh)I_{im}^*&0&0&0&0\\0&0&J_{i0}^*&J_{im}^*&0&0\\I_{im}^*&0&0&0&0&0\end{pmatrix},$$

where each element [such as $\cos(\mu_mh)J_{im}^*$] represents a matrix, and the multiplication such as $\cos(\mu_mh)J_{im}^*E_m^j$ in $P_1Z_m^j$ of Eq. (2.11) implies summation over the index ''m,'' which is just the multiplication of a matrix and a column vector. Here I_{im} and J_{im} are defined as $I_{im}=\int_0^a e^{ik_{ix}x}X_m(x)dx$ and $J_{im}=\int_0^a e^{ik_{ix}x}Y_m(x)dx$. When we match the boundary conditions for the magnetic field at the interfaces $z=h$ and $z=0$, we project both hand sides of Eq. (2.10b) and Eq. (2.10d) onto the basis of modal functions $X_m(x)$ and $Y_m(x)$. From this we obtain

$$ik_0P_2Z_1^j=P_3Z_m^j, \tag{2.12}$$

where

$$Z_1^j=[H_{ij,x}(h),H_{ij,y}(h),V_{ij,x}(0),V_{ij,y}(0)]^T.$$

P_2 is a $(4M-2)\times(4N_0)$ matrix defined by

$$P_2=\begin{pmatrix} I_{im} & 0 & 0 & 0\\ 0 & J_{im} & 0 & 0\\ 0 & J_{i0} & 0 & 0\\ 0 & 0 & I_{im} & 0\\ 0 & 0 & 0 & J_{i0}\\ 0 & 0 & 0 & J_{im}\end{pmatrix},$$

where I_{im} denotes a $(M-1)\times N_0$ matrix, and multiplication such as $I_{im}H_{ij,x}(h)$ in $P_2Z_1^j$ of Eq. (2.12) should be understood as the multiplication of a matrix and a column vector, on which summation over the index ''i'' is imposed. Others have similar implications.

P_3 is a $(4M-2)\times(4M-2)$ matrix defined by

$$P_3=\begin{pmatrix} Q_{11} & Q_{12} & 0 & Q_{14} & 0 & Q_{16}\\ Q_{21} & Q_{22} & 0 & Q_{24} & 0 & Q_{26}\\ 0 & 0 & Q_{33} & 0 & Q_{35} & 0\\ 0 & Q_{42} & 0 & 0 & 0 & Q_{46}\\ 0 & 0 & 0 & 0 & Q_{55} & 0\\ 0 & Q_{62} & 0 & 0 & 0 & Q_{66}\end{pmatrix},$$

where each block matrix Q_{ij} is diagonal. The diagonal elements are $Q_{11,mm}=(k_{jy}^2\mu_m^{-1}+\mu_m)\sin(\mu_m h)$, $Q_{12,mm}=-(k_{jy}^2\mu_m^{-1}+\mu_m)\cos(\mu_m h)$, $Q_{14,mm}=ik_{jy}\mu_m^{-1}s_m\sin(\mu_m h)$, $Q_{16,mm}=-ik_{jy}\mu_m^{-1}s_m\cos(\mu_m h)$, $Q_{21,mm}=ik_{jy}\mu_m^{-1}s_m\sin(\mu_m h)$, $Q_{22,mm}=-ik_{jy}\mu_m^{-1}s_m\cos(\mu_m h)$, $Q_{24,mm}=-(s_m^2 mu_m^{-1}+\mu_m)\sin(\mu_m h)$, $Q_{26,mm}=(s_m^2 mu_m^{-1}+\mu_m)\cos(\mu_m h)$, $Q_{33,mm}=-\mu_0\sin(\mu_0 h)$, $Q_{35,mm}=\mu_0\cos(\mu_0 h)$, $Q_{42,mm}=-(k_{jy}^2\mu_m^{-1}+\mu_m)$, $Q_{46,mm}=-ik_{jy}\mu_m^{-1}s_m$, $Q_{55,mm}=\mu_0$, $Q_{62,mm}=-ik_{jy}\mu_m^{-1}s_m$, and $Q_{66,mm}=s_m^2\mu_m^{-1}+\mu_m$.

To solve the transmission and reflection spectra, one can first delete the modal variables from Eqs. (2.11) and (2.12). This can be done by first calculating the inverse of P_3 by means of analytical manipulation, then substituting Z_m^j back into Eq. (2.11). We finally obtain the following linear equations satisfied by the plane-wave expansion coefficients:

$$Z_0^j=P^jZ_1^j, \tag{2.13}$$

where the $(4N_0)\times(4N_0)$ coefficient matrix reads

$$P^j=\begin{pmatrix} P_{11} & P_{12} & P_{13} & P_{14}\\ P_{21} & P_{22} & P_{23} & P_{24}\\ P_{31} & P_{32} & P_{33} & P_{34}\\ P_{41} & P_{42} & P_{43} & P_{44}\end{pmatrix}.$$

The block matrices $P_{ij}(i,j=1,4)$ each is of dimension $N_0\times N_0$. They are defined as

$$P_{11}^{ii'}=-(ik_0/d)\sum_{m=1}^{M-1}\operatorname{ctan}(\mu_m h)Z_m^{(21)}J_{im}^*I_{i'm},$$

$$P_{12}^{ii'}=-(ik_0/d)\mu_0^{-1}\operatorname{ctan}(\mu_0 h)J_{i0}^*J_{i'0}-(ik_0/d)\sum_{m=1}^{M-1}\operatorname{ctan}(\mu_m h)Z_m^{(22)}J_{im}^*J_{i'm},$$

$$P_{13}^{ii'}=(ik_0/d)\sum_{m=1}^{M-1}\csc(\mu_m h)Z_m^{(21)}J_{im}^*I_{i'm},$$

$$P_{14}^{ii'}=(ik_0/d)\mu_0^{-1}\csc(\mu_0 h)J_{i0}^*J_{i'0}-(ik_0/d)\sum_{m=1}^{M-1}\csc(\mu_m h)Z_m^{(22)}J_{im}^*J_{i'm},$$

$$P_{21}^{ii'}=-(ik_0/d)\sum_{m=1}^{M-1}\operatorname{ctan}(\mu_m h)Z_m^{(11)}I_{im}^*I_{i'm},$$

$$P_{22}^{ii'}=-(ik_0/d)\sum_{m=1}^{M-1}\operatorname{ctan}(\mu_m h)Z_m^{(12)}I_{im}^*J_{i'm},$$

$$P_{23}^{ii'}=(ik_0/d)\sum_{m=1}^{M-1}\csc(\mu_m h)Z_m^{(11)}I_{im}^*I_{i'm},$$

$$P_{24}^{ii'}=(ik_0/d)\sum_{m=1}^{M-1}\csc(\mu_m h)Z_m^{(12)}I_{im}^*J_{i'm},$$

where

$$Z_m^{(11)}=(s_m^2\mu_m^{-1}+\mu_m)/k_0^2,\quad Z_m^{(12)}=ik_{jy}\mu_m^{-1}s_m/k_0^2,$$

$$Z_m^{(21)}=-ik_{jy}\mu_m^{-1}s_m/k_0^2,\quad Z_m^{(22)}=-(k_{jy}^2\mu_m^{-1}+\mu_m)/k_0^2.$$

Other matrices are given according to the following symmetry relations

$$P_{31}^{ii'}=-P_{13}^{ii'},\quad P_{32}^{ii'}=-P_{14}^{ii'},$$

$$P_{33}^{ii'}=-P_{11}^{ii'},\quad P_{34}^{ii'}=-P_{12}^{ii'},$$

$$P_{41}^{ii'}=-P_{23}^{ii'},\quad P_{42}^{ii'}=-P_{24}^{ii'},$$

$$P_{43}^{ii'}=-P_{21}^{ii'},\quad P_{44}^{ii'}=-P_{22}^{ii'}.$$

Now inserting into Eq. (2.13) the definition of Z_0^j and Z_1^j with respect to $E_{ij,x}(h)$, $E_{ij,y}(h)$, $U_{ij,x}(0)$, $U_{ij,y}(0)$, $H_{ij,x}(h)$, $H_{ij,y}(h)$, $V_{ij,x}(0)$, and $V_{ij,y}(0)$, and using the relation between E_{ij} and H_{ij}, U_{ij}, and V_{ij}, we get

$$\begin{pmatrix}\psi_j^+\\ \chi_j^+\end{pmatrix}=\begin{pmatrix}P_{11}^jT_0^j & P_{12}^jT_0^j\\ P_{21}^jT_0^j & P_{22}^jT_0^j\end{pmatrix}\begin{pmatrix}\psi_j^-\\ \chi_j^-\end{pmatrix}, \tag{2.14}$$

where ψ_j^+, χ_j^+, ψ_j^-, and χ_j^- are $2N_0$-dimensioned column vectors defined by

$$\psi_j^+=(\ldots,E_{0j,x}^+,E_{0j,y}^+,\ldots,E_{ij,x}^+,E_{ij,y}^+,\ldots)^T+(\ldots,E_{0j,x}^-,E_{0j,y}^-,\ldots,E_{ij,x}^-,E_{ij,y}^-,\ldots)^T,$$

$$\psi_j^-=(\ldots,E_{0j,x}^+,E_{0j,y}^+,\ldots,E_{ij,x}^+,E_{ij,y}^+,\ldots)^T-(\ldots,E_{0j,x}^-,E_{0j,y}^-,\ldots,E_{ij,x}^-,E_{ij,y}^-,\ldots)^T,$$

$$\chi_j^+=(\ldots,U_{0j,x}^+,U_{0j,y}^+,\ldots,U_{ij,x}^+,U_{ij,y}^+,\ldots)^T+(\ldots,U_{0j,x}^-,U_{0j,y}^-,\ldots,U_{ij,x}^-,U_{ij,y}^-,\ldots)^T,$$

$$\chi_j^-=(\ldots,U_{0j,x}^+,U_{01j,y}^+,\ldots,U_{ij,x}^+,U_{ij,y}^+,\ldots)^T-(\ldots,U_{0j,x}^-,U_{0j,y}^-,\ldots,U_{ij,x}^-,U_{ij,y}^-,\ldots)^T.$$

The index i ranges inside $-N\leqslant i\leqslant N$. T_0^j is a $(2N_0\times 2N_0)$-dimensioned block-diagonal matrix consisting of $\{T_{0,ij},i=-N,N\}$ at its diagonal positions

$$T_0^j=\begin{pmatrix} T_{0,-Nj} & \cdots & 0 & \cdots & 0\\ \cdots & \cdots & \cdots & \cdots & \cdots\\ \cdots & 0 & T_{0,0j} & 0 & \cdots\\ \cdots & \cdots & \cdots & \cdots & \cdots\\ 0 & \cdots & 0 & \cdots & T_{0,Nj}\end{pmatrix}.$$

For a one-layer 1D grating slab, we recognize that $\psi_j^+=E_0^j+E_r^j$, $\psi_j^-=E_0^j-E_r^j$, $\chi_j^+=\chi_j^-=E_t^j$, where E_0^j, E_r^j, and E_t^j are column vectors consisting of the coefficients for the incident, reflected, and transmitted waves. Since in the usual diffraction problem only zero-order wave is incident on the grating, we can set $E_0^j=(0,0,\ldots,0,0,E_{0x},E_{0y},0,0,\ldots,0,0)$, where E_{0x} and E_{0y} are the amplitudes of the incident electric field components. From Eq. (2.14) we find that E_r^j and E_t^j satisfy

$$\begin{pmatrix} I+P_{11}^jT_0^j & -P_{12}^jT_0^j\\ P_{21}^jT_0^j & I-P_{22}^jT_0^j\end{pmatrix}\begin{pmatrix}E_r^j\\ E_t^j\end{pmatrix}=\begin{pmatrix} P_{11}^jT_0^j-I & P_{12}^jT_0^j\\ P_{21}^jT_0^j & P_{22}^jT_0^j-I\end{pmatrix}\begin{pmatrix}E_0^j\\ 0\end{pmatrix}=\begin{pmatrix}(P_{11}^jT_0^j-I)E_0^j\\ P_{21}^jT_0^jE_0^j\end{pmatrix}, \tag{2.15}$$

where I is a unit matrix. The simultaneous linear equations Eq. (2.15) can be solved via the standard Gaussian elimination method. Numerical experiences indicate that the numerical convergence for the off-plane scattering problem is as fast as for the in-plane incidence situation, where usage of 11 plane waves and 11 modes has already led to converged result of transmission and reflection spectra for both the TE and TM polarization modes. This verifies the powerful strength of this analytical modal method.

III. METALLIC LAYER-BY-LAYER PHOTONIC CRYSTAL GRATINGS IN MICROWAVE REGIMES

Now that we have developed a powerful tool which enables us to solve accurately and efficiently EM waves scattering by a 1D perfect-conducting grating under general incidence conditions, we can proceed to consider a more complex 2D layer-by-layer perfect-conducting photonic crystal grating, each layer of which is a 1D lamellar grating. A metallic grating working in the microwave regime can be assumed as a perfect-conducting grating. In this 2D structure, the EM fields should be projected onto the 2D plane-wave basis, namely, we have now $\mathbf{k}=(k_{ij,x},k_{ij,y},\beta_{ij})$, where $k_{ij,x}=k_{0x}+i2\pi/d$, $k_{ij,y}=k_{0y}+j2\pi/d$, $\beta_{ij}=-(k_0^2-k_{ij,x}^2-k_{ij,y}^2)^{1/2}$ for $k_0^2-k_{ij,x}^2-k_{ij,y}^2\geqslant 0$, and $\beta_{ij}=-i(k_{ij,x}^2+k_{ij,y}^2-k_0^2)^{1/2}$ for $k_0^2-k_{ij,x}^2-k_{ij,y}^2<0$. In principle, the indices i,j should both run from $-\infty$ to $+\infty$, but in practice, truncations must be used and we take $-N\leqslant i\leqslant N$ and $-N\leqslant j\leqslant N$ where N is an integer number. Let $N_0=2N+1$, the total plane wave number is then N_0^2. The EM fields are expanded into

$$\mathbf{E}(\mathbf{r})=\sum_{i,j}\mathbf{E}_{ij}(z)e^{ik_{ij,x}x+ik_{ij,y}y}, \tag{3.1}$$

$$\mathbf{H}(\mathbf{r})=\sum_{i,j}\mathbf{H}_{ij}(z)e^{ik_{ij,x}x+ik_{ij,y}y}. \tag{3.2}$$

As we have noted in Sec. II, each layer is a 1D grating, so the wave vector parallel to the axis of this 1D grating is kept constant. This means we can directly utilize the result for 1D gratings developed in Sec. II. For the layer in which the rods are along the y axis, we rewrite the EM fields into

$$\mathbf{E}(\mathbf{r})=\sum_{j=-\infty}^{\infty}\left[\sum_{i=-\infty}^{\infty}\mathbf{E}_{ij}(z)e^{ik_{ij,x}x}e^{ik_{ij,y}y}\right], \tag{3.3}$$

$$\mathbf{H}(\mathbf{r})=\sum_{j=-\infty}^{\infty}\left[\sum_{i=-\infty}^{\infty}\mathbf{H}_{ij}(z)e^{ik_{ij,x}x}e^{ik_{ij,y}y}\right]. \tag{3.4}$$

Each term inside the bracket "[ ]" has the same form as Eqs. (2.1) and (2.2), whose solutions we have known in Sec. II. Therefore, we can directly write down the following matrix equation for the tangential components of the EM fields as

$$\begin{pmatrix}\Omega_0^+\\ \Omega_1^+\end{pmatrix}=\begin{pmatrix} r_{11} & r_{12}\\ r_{21} & r_{22}\end{pmatrix}\begin{pmatrix}\Omega_0^-\\ \Omega_1^-\end{pmatrix}, \tag{3.5}$$

where Ω_0^+, Ω_1^+, Ω_0^-, and Ω_1^- are now $2N_0^2$-dimensioned column vectors defined by

$$\Omega_0^+=(\psi_{-N}^+,\ldots,\psi_0^+,\ldots,\psi_N^+)^T,$$

$$\Omega_0^-=(\psi_{-N}^-,\ldots,\psi_0^-,\ldots,\psi_N^-)^T,$$

$$\Omega_1^+=(\chi_{-N}^+,\ldots,\chi_0^+,\ldots,\chi_N^+)^T,$$

$$\Omega_1^-=(\chi_{-N}^-,\cdots,\chi_0^-,\cdots,\chi_N^-)^T.$$

$r_{mn}(m,n=1,2)$ is each a $(2N_0^2)\times(2N_0^2)$ block-diagonal matrix, which are defined as

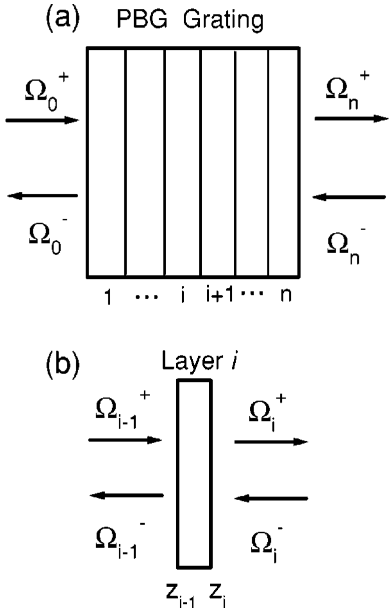

FIG. 3. (a) Schematical configuration of a multilayer layer-by-layer photonic crystal grating. An overall R matrix can be defined connecting the waves in the incident region ($\Omega_0^\pm$) and the transmission region ($\Omega_n^\pm$) in the transfer-matrix method for this multilayer grating. (b) A R matrix can be defined for a single layer of the layer-by-layer photonic crystal grating.

$$r_{mn}=\begin{pmatrix} P_{mn}^{-N}T_0^{-N} & \cdots & 0 & \cdots & 0 \\ \cdots & \cdots & \cdots & \cdots & \cdots \\ \cdots & 0 & P_{mn}^0 T_0^0 & 0 & \cdots \\ \cdots & \cdots & \cdots & \cdots & \cdots \\ 0 & \cdots & 0 & \cdots & P_{mn}^N T_0^N \end{pmatrix}.$$

One can recognize that the matrices r_{mn} are the so-called R matrix familiar to the grating community.[20,28] This is one of several powerful numerical techniques that can treat the scattering of EM waves by a grating with arbitrarily large thickness in a numerically stable manner.

When we deal with a grating consisting of many layers, as schematically depicted in Fig. 3(a), we can assume that each layer is surrounded by two imaginary infinitely-thin air films in its both sides, as displayed in Fig. 3(b). Now there is an overall R matrix connecting waves in the incident and transmission region of the multilayer grating. Furthermore, we can define a R matrix for each layer, as we have done in the above for a single-layer lamellar grating. The introduction of these extra air thin films generates no physical contamination to the scattering problem, because the thickness of all films is set to zero, and because the tangential components of the EM fields are continuous at the interface. But these imaginary air films will enable us to treat each grating layer separately in a systematical manner. All that leave is to combine all these single layers into a whole. Great convenience and flexibility are a natural result brought from such a technique. To appreciate the numerical stability for arbitrarily thick gratings, we use the R-matrix recursion algorithm[20,28] to calculate the overall R matrix connecting the plane waves in the incidence and transmission regions. The key point of this technique is as follows. Suppose we have obtained via numerical calculations the overall R matrix for the first n layers $R^{(n)}=(R_{11}^{(n)},R_{12}^{(n)},R_{21}^{(n)},R_{22}^{(n)})$, which satisfies

$$\begin{pmatrix} \Omega_0^+ \\ \Omega_n^+ \end{pmatrix}=\begin{pmatrix} R_{11}^{(n)} & R_{12}^{(n)} \\ R_{21}^{(n)} & R_{22}^{(n)} \end{pmatrix}\begin{pmatrix} \Omega_0^- \\ \Omega_n^- \end{pmatrix}, \tag{3.6}$$

and the R matrix $r^{(n+1)}$ for the $(n+1)_{th}$ layer, which satisfies

$$\begin{pmatrix} \Omega_n^+ \\ \Omega_{n+1}^+ \end{pmatrix}=\begin{pmatrix} r_{11}^{(n+1)} & r_{12}^{(n+1)} \\ r_{21}^{(n+1)} & r_{22}^{(n+1)} \end{pmatrix}\begin{pmatrix} \Omega_n^- \\ \Omega_{n+1}^- \end{pmatrix}, \tag{3.7}$$

where $\Omega_0^+(\Omega_0^-)$ and $\Omega_n^+(\Omega_n^-)$ are column vectors for waves in the upper side of the 1st and $(n+1)_{th}$ layer of the grating, while $\Omega_1^+(\Omega_1^-)$ and $\Omega_{n+1}^+(\Omega_{n+1}^-)$ are column vectors for waves in the lower side. We can straightforwardly prove that the overall R-matrix $R^{(n+1)}$ for the total $n+1$ layers is given by the following recursion formula

$$R_{11}^{(n+1)}=R_{11}^{(n)}+R_{12}^{(n)}[r_{11}^{(n+1)}-R_{22}^{(n)}]^{-1}R_{21}^{(n)}, \tag{3.8a}$$

$$R_{12}^{(n+1)}=-R_{12}^{(n)}[r_{11}^{(n+1)}-R_{22}^{(n)}]^{-1}r_{12}^{(n+1)}, \tag{3.8b}$$

$$R_{21}^{(n+1)}=r_{21}^{(n+1)}[r_{11}^{(n+1)}-R_{22}^{(n)}]^{-1}R_{21}^{(n)}, \tag{3.8c}$$

$$R_{22}^{(n+1)}=r_{22}^{(n+1)}-r_{21}^{(n+1)}[r_{11}^{(n+1)}-R_{22}^{(n)}]^{-1}r_{12}^{(n+1)}. \tag{3.8d}$$

Therefore, the procedure to calculate the overall R matrix for a grating can be summarized as follows: First calculate the R matrix for the first layer $r^{(1)}$ and set $R^{(1)}=r^{(1)}$. Then calculate the R matrix for the second layer $r^{(2)}$, and use the recursion algorithm Eqs. (3.8a)–(3.8d) to calculate the overall R matrix $R^{(2)}$ for the first two layers. Repeat this procedure until the final layer of the grating.

With the final overall R matrix at hand, we can solve the reflection and transmission coefficients by

$$\begin{pmatrix} E_0+E_r \\ E_t \end{pmatrix}=\begin{pmatrix} R_{11}^{(n+1)} & R_{12}^{(n+1)} \\ R_{21}^{(n+1)} & R_{22}^{(n+1)} \end{pmatrix}\begin{pmatrix} E_0-E_r \\ E_t \end{pmatrix} \tag{3.9}$$

or finally

$$\begin{pmatrix} I+R_{11}^{(n+1)} & -R_{12}^{(n+1)} \\ R_{21}^{(n+1)} & I-R_{22}^{(n+1)} \end{pmatrix}\begin{pmatrix} E_r \\ E_t \end{pmatrix}=\begin{pmatrix} (R_{11}^{(n+1)}-I)E_0 \\ R_{21}^{(n+1)}E_0 \end{pmatrix}. \tag{3.10}$$

Here I is an unit matrix, and

$$E_0=(E_{-N}^0,\dots,E_0^0,\dots,E_j^0,\dots,E_N^0)^T,$$

$$E_r=(E_{-N}^r,\dots,E_0^r,\dots,E_j^r,\dots,E_N^r)^T,$$

$$E_t=(E_{-N}^t,\dots,E_0^t,\dots,E_j^t,\dots,E_N^t)^T.$$

Each component E_j^0 etc. is a column vector, defined by

$$E_j^0=(E^0_{-Nj,x},E^0_{-Nj,y},\ldots,E^0_{0j,x},E^0_{0j,y},\ldots,E^0_{ij,x},E^0_{ij,y},\ldots,E^0_{Nj,x},E^0_{Nj,y})^T,$$

$$E_j^r=(E^r_{-Nj,x},E^r_{-Nj,y},\ldots,E^r_{0j,x},E^r_{0j,y},\ldots,E^r_{ij,x},E^r_{ij,y},\ldots,E^r_{Nj,x},E^r_{Nj,y})^T,$$

$$E_j^t=(E^t_{-Nj,x},E^t_{-Nj,y},\ldots,E^t_{0j,x},E^t_{0j,y},\ldots,E^t_{ij,x},E^t_{ij,y},\ldots,E^t_{Nj,x},E^t_{Nj,y})^T,$$

and so on. Notice $-N\leqslant i,j\leqslant N$. Obviously, here we have selected an index sequence of (j,i) to designate the plane wave components $(k_{ij,x},k_{ij,y})$. All numerical manipulations take this sequence as the universal basis.

Until now we have only derived the R matrix for the first layer of the photonic crystal grating, in which the rods are parallel to the y axis. Under a proper plane-wave basis, the R matrix is block diagonal. We can follow the same procedure to calculate the R matrix for the second layer, and other layers, but generally they do not appreciate the superior feature of a block-diagonal matrix. However, the symmetry of the photonic crystal grating suggests that we adopt an easier way to obtain the R matrix for other layers. We see that the second layer, with rods parallel to the x axis, is just a 90° rotation from the first layer. The third layer is translated by $d/2$ from the first layer along the x axis, and the fourth layer is translated from the second layer by $d/2$ along the y axis. In another words, the third and fourth layers as a whole are translated from the first and second layers by $(d/2,\ d/2)$. Therefore, under a straightforward transformation of coordinates, we can derive the R matrix for any layer in a much simpler way.

Let's first consider the 90° rotation transformation. The coordinates is transformed as

$$y\rightarrow x',\quad x\rightarrow -y', \tag{3.11}$$

where x,y and x',y' are coordinates in the lab (original) and crystal (rotated) frames. It also means that both the wave vectors and the amplitude of the EM field vectors should be transformed in the same way,

$$(k_x,k_y)\rightarrow(-k'_y,k'_x),\quad (E_x,E_y)\rightarrow(-E'_y,E'_x). \tag{3.12}$$

Suppose r' and r are the R matrix in the rotated and original coordinates, respectively. Let us write down Eq. (3.5) in a more explicit form for the two tangential components of the fields E_x and E_y:

$$\begin{pmatrix}\Omega'^{+}_{0x}(k'_{i,j})\\ \Omega'^{+}_{0y}(k'_{i,j})\\ \Omega'^{+}_{1x}(k'_{i,j})\\ \Omega'^{+}_{1y}(k'_{i,j})\end{pmatrix}=\begin{pmatrix} r'^{(11)}_{11} & r'^{(12)}_{11} & r'^{(11)}_{12} & r'^{(12)}_{12}\\ r'^{(21)}_{11} & r'^{(22)}_{11} & r'^{(21)}_{12} & r'^{(22)}_{12}\\ r'^{(11)}_{21} & r'^{(12)}_{21} & r'^{(11)}_{22} & r'^{(12)}_{12}\\ r'^{(21)}_{21} & r'^{(22)}_{21} & r'^{(21)}_{22} & r'^{(22)}_{12}\end{pmatrix}\times\begin{pmatrix}\Omega'^{-}_{0x}(k'_{m,n})\\ \Omega'^{-}_{0y}(k'_{m,n})\\ \Omega'^{-}_{1x}(k'_{m,n})\\ \Omega'^{-}_{1y}(k'_{m,n})\end{pmatrix} \tag{3.13}$$

and

$$\begin{pmatrix}\Omega^{+}_{0x}(k_{i,j})\\ \Omega^{+}_{0y}(k_{i,j})\\ \Omega^{+}_{1x}(k_{i,j})\\ \Omega^{+}_{1y}(k_{i,j})\end{pmatrix}=\begin{pmatrix} r^{(11)}_{11} & r^{(12)}_{11} & r^{(11)}_{12} & r^{(12)}_{12}\\ r^{(21)}_{11} & r^{(22)}_{11} & r^{(21)}_{12} & r^{(22)}_{12}\\ r^{(11)}_{21} & r^{(12)}_{21} & r^{(11)}_{22} & r^{(12)}_{12}\\ r^{(21)}_{21} & r^{(22)}_{21} & r^{(21)}_{22} & r^{(22)}_{12}\end{pmatrix}\begin{pmatrix}\Omega^{-}_{0x}(k_{m,n})\\ \Omega^{-}_{0y}(k_{m,n})\\ \Omega^{-}_{1x}(k_{m,n})\\ \Omega^{-}_{1y}(k_{m,n})\end{pmatrix}. \tag{3.14}$$

Here the subscript ''ij'' $(i,j=1,2)$ denote four block submatrices of the R matrix, while the superscript ''ij'' $(i,j=1,2)$ are for the x and y components of the electric field. $r'^{(11)}_{11}=r'^{(11)}_{11}(i,j;m,n)$, etc., are matrix elements of the R matrix in which the indices i,j,m,n have been neglected. Transforming Eq. (3.14) into the rotated coordinates, we have

$$\begin{pmatrix}-\Omega'^{+}_{0y}(k'_{-j,i})\\ \Omega'^{+}_{0x}(k'_{-j,i})\\ -\Omega'^{+}_{1y}(k'_{-j,i})\\ \Omega'^{+}_{1x}(k'_{-j,i})\end{pmatrix}=\begin{pmatrix} r^{(11)}_{11} & r^{(12)}_{11} & r^{(11)}_{12} & r^{(12)}_{12}\\ r^{(21)}_{11} & r^{(22)}_{11} & r^{(21)}_{12} & r^{(22)}_{12}\\ r^{(11)}_{21} & r^{(12)}_{21} & r^{(11)}_{22} & r^{(12)}_{12}\\ r^{(21)}_{21} & r^{(22)}_{21} & r^{(21)}_{22} & r^{(22)}_{12}\end{pmatrix}\times\begin{pmatrix}-\Omega'^{-}_{0y}(k'_{-n,m})\\ \Omega'^{-}_{0x}(k'_{-n,m})\\ -\Omega'^{-}_{1y}(k'_{-n,m})\\ \Omega'^{-}_{1x}(k'_{-n,m})\end{pmatrix}. \tag{3.15}$$

Note that $k_{i,j}$ in Eq. (3.14) is a compact form of $(k_{ij,x},k_{ij,y})=(k_{0x}+i2\pi/d,k_{0y}+j2\pi/d)$. When transformed into the new coordinate, it becomes $(-k'_{ij,y},k'_{ij,x})=(-k'_{0y}-j2\pi/d,k'_{0x}+i2\pi/d)$, which is written into a compact form of $k'_{-j,i}$ in Eq. (3.15). Here the Bloch's wave vector (k_{0x},k_{0y}) is also transformed into $(-k'_{0y},k'_{0x})$. Similarly, $k'_{i,j}$ in Eq. (3.13) is a compact form of $(k'_{ij,x},k'_{ij,y})=(-k'_{0y}+i2\pi/d,k'_{0x}+j2\pi/d)$. Comparing Eq. (3.15) with Eq. (3.13), we obtain the following transformation of the R matrix under a 90° coordinate rotation:

$$\begin{aligned} r'^{(22)}_{11}(-j,i;-n,m)&\rightarrow r^{(11)}_{11}(i,j;m,n),\\ -r'^{(21)}_{11}(-j,i;-n,m)&\rightarrow r^{(12)}_{11}(i,j;m,n),\\ -r'^{(12)}_{11}(-j,i;-n,m)&\rightarrow r^{(21)}_{11}(i,j;m,n),\\ r'^{(11)}_{11}(-j,i;-n,m)&\rightarrow r^{(22)}_{11}(i,j;m,n). \end{aligned} \tag{3.16}$$

The same transformation rule applies to other block submatrices r_{12}, r_{21}, and r_{22}.

The transformation of the R matrix under a coordinate translation is much simpler compared to the transformation under a coordinate rotation. Under axis translation

$$x\rightarrow x'-x_0,\quad y\rightarrow y'-y_0, \tag{3.17}$$

the field amplitudes (including directions) and Bragg wave vectors keep unchanged

$$(k_x,k_y)\rightarrow(k'_x,k'_y),\quad (E_x,E_y)\rightarrow(E'_x,E'_y). \tag{3.18}$$

Each plane-wave component of the electric field is transformed according to $E(k_{i,j})e^{ik_ix+ik_j}\rightarrow E'(k'_{i,j})e^{ik'_ix'+ik'_jy'}=E'(k'_{i,j})e^{ik_ix+ik_jy}e^{-ik_ix_0-ik_jy_0}$. This leads to

$$E(k_{i,j})\rightarrow E'(k'_{i,j})e^{-ik_ix_0-ik_jy_0}. \tag{3.19}$$

Looking into the definition of the R matrix, we find the following transformation of the R matrix under a coordinate translation:

$$r'_{11}(i,j;m,n)e^{i(k_m-k_i)x_0+i(k_n-k_j)y_0}\rightarrow r_{11}(i,j;m,n), \tag{3.20}$$

and r_{12}, r_{21}, and r_{22} follow the same transformation rule.

According to the above analysis, we see that if the EM wave is normally incident on the 2D grating, then the R matrix of the second layer is just a 90° coordinate-rotation transformation from that for the first layer, which is block diagonal. The R matrix for the third and fourth layers are obtained by performing a coordinate-translation transformation over the R matrix for the first and second layer, respectively. Therefore, in this normal incident situation, only the R matrix for the first layer is needed. This greatly releases the numerical efforts. The overall R matrix for the 2D photonic crystal grating with arbitrary layers can be calculated on the basis of the first layer using the R matrix recursion algorithm shown in Eq. (3.8). For arbitrary incidence angles, the R matrix of the second layer is no longer a simple coordinate-rotation transformation from the first layer. Instead, we should first make a transformation so that in the 90°-rotated coordinate the incident wave vector witnessed by the second layer is $(k'_{0x},k'_{0y})=(-k_{0y},k_{0x})$. Then we calculate the R matrix r' (which is block diagonal) in this rotated coordinate using the same procedure for the first layer. Finally we back transform this block-diagonal matrix to obtain the R matrix r in the original coordinate according to Eq. (3.16). As a comparison, it is obvious that the transformation rule under a coordinate translation keeps the same for any incident angle, whether normal or not.

After we have obtained the coefficients for the reflection and transmission waves, the transmission and reflection coefficients are calculated by

$$T=\sum_{ij} T_{ij}=\sum_{ij}\frac{|\mathbf{E}^t_{ij}|^2|k_{ij,z}|}{|\mathbf{E}_0|^2|k_{0z}|} \tag{3.21}$$

and

$$R=\sum_{ij} R_{ij}=\sum_{ij}\frac{|\mathbf{E}^r_{ij}|^2|k_{ij,z}|}{|\mathbf{E}_0|^2|k_{0z}|}, \tag{3.22}$$

where the summation is run over those homogeneous Bragg waves with a lateral wave vector $[k_{0x}+i(2\pi/d)]^2+[k_{0y}+j(2\pi/d)]^2\leqslant k_0^2$. $\mathbf{E}^t_{ij}$ and $\mathbf{E}^r_{ij}$ are the amplitudes of the transmission and reflection Bragg wave in the $(ij)_{th}$ order, respectively.

IV. METALLIC LAYER-BY-LAYER PHOTONIC CRYSTAL GRATINGS IN MIDINFRARED REGIMES

When a metallic grating is working in the mid-IR regime, the metal is finite conducting but has a very small skin depth. We can still use the analytic modal method to solve the scattering problem by such a highly-conducting layer-by-layer grating, however, the solution now becomes much more complicated.

The key point is to solve the eigenmodes inside each 1D lamellar grating under arbitrary incident conditions. To achieve this, we use the following trial function as an eigenmode in a metallic grating consisting of infinitely-long rectangular rods along the y-axis direction,

$$E_y(\mathbf{r})=e^{ik_zz+ik_yy}[A_1\sin(\beta_1x)+B_1\cos(\beta_1x)], \tag{4.1}$$

$$E_z(\mathbf{r})=e^{ik_zz+ik_yy}[C_1\sin(\beta_1x)+D_1\cos(\beta_1x)], \tag{4.2}$$

$$\begin{aligned}E_x(\mathbf{r})=e^{ik_zz+ik_yy}[&-(ik_yB_1+ik_zD_1)\beta_1^{-1}\sin(\beta_1x)\\&+(ik_yA_1+ik_zB_1)\beta_1^{-1}\cos(\beta_1x)],\end{aligned} \tag{4.3}$$

$$\begin{aligned}ik_0H_y(\mathbf{r})=e^{ik_zz+ik_yy}[&k_z(k_yB_1+k_zD_1)\beta_1^{-1}\sin(\beta_1x)\\&-k_z(k_yA_1+k_zC_1)\beta_1^{-1}\cos(\beta_1x)\\&-\beta_1C_1\cos(\beta_1x)+\beta_1D_1\sin(\beta_1x)],\end{aligned} \tag{4.4}$$

$$\begin{aligned}ik_0H_z(\mathbf{r})=e^{ik_zz+ik_yy}[&-k_y(k_yB_1+k_zD_1)\beta_1^{-1}\sin(\beta_1x)\\&+k_y(k_yA_1+k_zC_1)\beta_1^{-1}\cos(\beta_1x)\\&+\beta_1A_1\cos(\beta_1x)-\beta_1B_1\sin(\beta_1x)],\end{aligned}$$

$$\begin{aligned}ik_0H_x(\mathbf{r})=e^{ik_zz+ik_yy}[&(ik_yC_1-ik_zA_1)\sin(\beta_1x)\\&+(ik_yD_1-ik_zB_1)\cos(\beta_1x)],\end{aligned} \tag{4.5}$$

for the E field and H fields in the air domain $0\leqslant x<a$. Here $k_z^2+\beta_1^2+k_y^2=\epsilon_1k_0^2$, $\mathrm{Im}(\beta_1)>0$, and $\epsilon_1=1$ is the dielectric constant of the air domain. The EM fields in the metal domain $a\leqslant x<d$ are

$$E_y(\mathbf{r})=e^{ik_zz+ik_yy}[A_2e^{i\beta_2(x-a)}+B_2e^{-i\beta_2(x-d)}], \tag{4.6}$$

$$E_z(\mathbf{r})=e^{ik_zz+ik_yy}[C_2e^{i\beta_2(x-a)}+D_2e^{-i\beta_2(x-d)}], \tag{4.7}$$

$$\begin{aligned}E_x(\mathbf{r})=e^{ik_zz+ik_yy}[&-(k_yA_2+k_zC_2)\beta_2^{-1}e^{i\beta_2(x-a)}\\&+(k_yB_2+k_zD_2)\beta_2^{-1}e^{-i\beta_2(x-d)}],\end{aligned} \tag{4.8}$$

$$\begin{aligned}ik_0H_y(\mathbf{r})=e^{ik_zz+ik_yy}[&-ik_yk_z\beta_2^{-1}A_2e^{i\beta_2(x-a)}\\&+ik_yk_z\beta_2^{-1}B_2e^{-i\beta_2(x-d)}\\&-(ik_z^2\beta_2^{-1}+i\beta_2)C_2e^{i\beta_2(x-a)}\\&+(ik_z^2\beta_2^{-1}+i\beta_2)D_2e^{-i\beta_2(x-d)}],\end{aligned} \tag{4.9}$$

$$
\begin{aligned}
ik_0H_z(\mathbf{r}) = e^{ik_zz+ik_yy}[& ik_yk_z\beta_2^{-1}C_2e^{i\beta_2(x-a)} \\
& -ik_yk_z\beta_2^{-1}D_2e^{-i\beta_2(x-d)} \\
& +(ik_y^2\beta_2^{-1}+i\beta_2)A_2e^{i\beta_2(x-a)} \\
& -(ik_y^2\beta_2^{-1}+i\beta_2)B_2e^{-i\beta_2(x-d)}],
\end{aligned} \tag{4.10}
$$

$$
\begin{aligned}
ik_0H_x(\mathbf{r}) = e^{ik_zz+ik_yy}[& (ik_yC_2-ik_zA_2)e^{i\beta_2(x-a)} \\
& +(ik_yD_2-ik_zB_2)e^{-i\beta_2(x-d)}].
\end{aligned} \tag{4.11}
$$

Here $k_z^2+\beta_2^2+k_y^2=\epsilon_2k_0^2$, $\mathrm{Im}(\beta_2)>0$, and ϵ_2 is the dielectric constant of the metal domain, which has strong dispersion. In writing down the above trial solution, we have noticed that k_z is a tangential wave vector component along the metal wall, and assumed to be invariant across this air-metal interface in order to match the boundary condition at the interface.

To determine the amplitudes in the trial solution, boundary conditions at metal walls located at $x=a$ and $x=d$ are used. E_y, E_z, H_y and H_z are continuous across the metal walls. So we have

$$A_1\sin(\beta_1a)+B_1\cos(\beta_1a)=A_2, \tag{4.12}$$

$$C_1\sin(\beta_1a)+D_1\cos(\beta_1a)=C_2, \tag{4.13}$$

$$p_0B_1=B_2, \tag{4.14}$$

$$p_0D_1=D_2, \tag{4.15}$$

for the E-field continuity, where $p_0=e^{ik_{0x}d}$ is the Bloch's phase factor. In deriving Eqs. (4.14) and (4.15), we have used Bloch's theorem to relate fields at $x=0$ and $x=d$. In addition, we have neglected terms with a factor $e^{i\beta_2(d-a)}$, which is a small number due to the far larger metal domain width compared to the skin depth of metal in the midinfrared wavelength regime. The continuity of the H field leads to

$$
\begin{aligned}
& -k_yk_z\beta_1^{-1}\cos(\beta_1a)A_1+k_yk_z\beta_1^{-1}\sin(\beta_1a)B_1 \\
& \quad -(k_z^2\beta_1^{-1}+\beta_1)\cos(\beta_1a)C_1+(k_z^2\beta_1^{-1}+\beta_1)\sin(\beta_1a)D_1 \\
& \quad =-ik_yk_z\beta_2^{-1}A_2-(k_z^2\beta_2^{-1}+\beta_2)C_2,
\end{aligned} \tag{4.16}
$$

$$
\begin{aligned}
& k_yk_z\beta_1^{-1}\cos(\beta_1a)C_1-k_yk_z\beta_1^{-1}\sin(\beta_1a)D_1 \\
& \quad +(k_y^2\beta_1^{-1}+\beta_1)\cos(\beta_1a)A_1-(k_y^2\beta_1^{-1}+\beta_1)\sin(\beta_1a)B_1 \\
& \quad =ik_yk_z\beta_2^{-1}B_2+(k_y^2\beta_2^{-1}+\beta_2)D_2,
\end{aligned} \tag{4.17}
$$

$$
\begin{aligned}
& p_0[-k_yk_z\beta_1^{-1}A_1-(k_z^2\beta_1^{-1}+\beta_1)C_1] \\
& \quad =ik_yk_z\beta_2^{-1}B_2+(k_z^2\beta_2^{-1}+\beta_2)D_2,
\end{aligned} \tag{4.18}
$$

$$
\begin{aligned}
& p_0[k_yk_z\beta_1^{-1}C_1-(k_y^2\beta_1^{-1}+\beta_1)A_1] \\
& \quad =-ik_yk_z\beta_2^{-1}D_2-(k_y^2\beta_2^{-1}+\beta_2)B_2.
\end{aligned} \tag{4.19}
$$

Defining 2×2 matrices

$$T_1=\begin{bmatrix} -k_yk_z\beta_1^{-1} & -(k_z^2\beta_1^{-1}+\beta_1) \\ k_y^2\beta_1^{-1}+\beta_1 & k_yk_z\beta_1^{-1} \end{bmatrix} \tag{4.20}$$

and

$$T_2=\begin{bmatrix} -ik_yk_z\beta_2^{-1} & -i(k_z^2\beta_2^{-1}+\beta_2) \\ i(k_y^2\beta_2^{-1}+\beta_2) & ik_yk_z\beta_2^{-1} \end{bmatrix}, \tag{4.21}$$

we can derive from Eqs. (4.12)–(4.19) the following equations:

$$\begin{pmatrix} A_2 \\ C_2 \end{pmatrix}=T_2^{-1}T_1\begin{pmatrix} A_1 \\ C_1 \end{pmatrix}\cos(\beta_1a)-T_2^{-1}T_1\begin{pmatrix} B_1 \\ D_1 \end{pmatrix}\sin(\beta_1a), \tag{4.22}$$

$$\begin{pmatrix} A_2 \\ C_2 \end{pmatrix}=\begin{pmatrix} A_1 \\ C_1 \end{pmatrix}\sin(\beta_1a)+\begin{pmatrix} B_1 \\ D_1 \end{pmatrix}\cos(\beta_1a), \tag{4.23}$$

$$\begin{pmatrix} B_1 \\ D_1 \end{pmatrix}=-T_2^{-1}T_1\begin{pmatrix} A_1 \\ C_1 \end{pmatrix}. \tag{4.24}$$

Designating $T=T_2^{-1}T_1$, and deleting B_1 and D_1 from Eqs. (4.22)–(4.24), we finally have

$$(I-T^2)\begin{pmatrix} A_1 \\ C_1 \end{pmatrix}\sin(\beta_1a)=2T\begin{pmatrix} A_1 \\ C_1 \end{pmatrix}\cos(\beta_1a), \tag{4.25}$$

$$\mathrm{tg}(\beta_1a)\begin{pmatrix} A_1 \\ C_1 \end{pmatrix}=2(I-T^2)^{-1}T\begin{pmatrix} A_1 \\ C_1 \end{pmatrix}. \tag{4.26}$$

Equation (4.26) is recognized to be a standard eigenequation for the matrix $Q=2(I-T^2)^{-1}T$, with $\mathrm{tg}(\beta_1a)$ being the eigenvalue. It will be shown that this eigenequation can be analytically solved. Notice Q and T has the same eigenvector, it suffices to work on T, whose explicit form is

$$T=T_2^{-1}T_1=\frac{-i}{\epsilon_2k_0^2}\begin{bmatrix} k_z^2\beta_2^{-1}\beta_1+k_y^2\beta_2\beta_1^{-1}+\beta_1\beta_2 & k_yk_z(\beta_1^{-1}\beta_2-\beta_2^{-1}\beta_1) \\ k_yk_z(\beta_1^{-1}\beta_2-\beta_2^{-1}\beta_1) & k_y^2\beta_2^{-1}\beta_1+k_z^2\beta_2\beta_1^{-1}+\beta_1\beta_2 \end{bmatrix}. \tag{4.27}$$

After some algebraic manipulations, we find that the eigenequation

$$T\begin{pmatrix} A_1 \\ C_1 \end{pmatrix} = x\begin{pmatrix} A_1 \\ C_1 \end{pmatrix} \tag{4.28}$$

has eigenvalues of $x=-i\epsilon_1\beta_2/\epsilon_2\beta_1$ and $x=-i\beta_1/\beta_2$, corresponding to eigenvectors $(A_1,C_1)=(1,-k_y/k_z)$ and $(A_1,C_1)=(k_y/k_z,1)$, respectively. From this, the eigenvalues of Eq. (4.26) are directly calculated as

$$\mathrm{tg}(\beta_1 a)=\frac{-2i\beta_1\beta_2}{\beta_1^2+\beta_2^2} \tag{4.29}$$

and

$$\mathrm{tg}(\beta_1 a)=\frac{-2i\epsilon_1\epsilon_2\beta_1\beta_2}{\epsilon_2^2\beta_1^2+\epsilon_1^2\beta_2^2}. \tag{4.30}$$

The corresponding eigenvectors are still $(A_1^1,C_1^1)=(1,-k_y/k_z)$ and $(A_1^2,C_1^2)=(k_y/k_z,1)$, respectively. We have designated these two modes as mode 1 and mode 2. Equations (4.29) and (4.30) are both complex transcendent equations with an infinite number of roots in the complex plane, which need to be numerically solved by searching the whole complex plane. To avoid this numerical difficulty, we start from solutions for a perfect-conducting metal wall. We keep in mind that with a large number of ϵ_2 in the midinfrared regime, the eigenmodes within the grating should not depart far away from those within the corresponding perfect-conducting structure, which we have known in the above sections. Therefore, we can use simple iteration techniques to find the accurate solutions of β_1 in Eqs. (4.29) and (4.30). For higher modes $m\geqslant 1$, we set the initial value of β_1 to be $\beta_1^{(0)}=s_m$, then the following iteration algorithm is followed:

$$\mathrm{tg}[\beta_1^{(n+1)}a]=\frac{-2i\beta_1^{(n)}\beta_2^{(n)}}{[\beta_1^{(n)}]^2+[\beta_2^{(n)}]^2}, \tag{4.31}$$

$$\mathrm{tg}[\beta_1^{(n+1)}a]=\frac{-2i\epsilon_1\epsilon_2\beta_1^{(n)}\beta_2^{(n)}}{\epsilon_2^2[\beta_1^{(n)}]^2+\epsilon_1^2[\beta_2^{(n)}]^2}, \tag{4.32}$$

where $n=0,1,2,\ldots,$ $[\beta_2^{(n)}]^2=(\epsilon_2-\epsilon_1)k_0^2+[\beta_1^{(n)}]^2$. In practice, several iteration loops are enough to bring us to a convergent solution of β_1 with considerable accuracy. Every solution corresponds to a fixed point $\beta_1^{(n+1)}=\beta_1^{(n)}$, and good convergence is due to the correct guess of initial value from physical consideration.

The iteration technique can not be applied to the lowest mode by starting from $\beta_1^{(0)}=s_0=0$. It is easy to find that $\beta_1=0$ is a solution of both Eqs. (4.29) and (4.30). However, it can be shown that this solution is unphysical unless ϵ_2 is infinite. Since Eq. (4.28) has only solution of $\beta_1=0$, it is excluded. Noticing that β_1 is a small number, we find from Eq. (4.30) as an approximation the following formula:

$$\beta_1 a=\frac{-2i\epsilon_1\epsilon_2\beta_1\beta_2}{\epsilon_2^2\beta_1^2+\epsilon_1^2\beta_2^2}, \tag{4.33}$$

whose nonzero solution is $\beta_1=\{-[a\epsilon_1^2(\beta_2^{(0)})^2+2i\beta_2^{(0)}\epsilon_1\epsilon_2]/[a\epsilon_2^2]\}^{1/2}$, where $\beta_2^{(0)}=(\epsilon_2-\epsilon_1)^{1/2}k_0$. To improve the accuracy of solution, we can do search in a small region on the complex plane around $\beta_1=\{-[a\epsilon_1^2(\beta_2^{(0)})^2+2i\beta_2^{(0)}\epsilon_1\epsilon_2]/[a\epsilon_2^2]\}^{1/2}$.

What happens if ϵ_2 is infinite? Obviously, for the lowest mode, $\beta_1\to 0$. For higher modes, we have double-degenerate solutions as $\mathrm{tg}(\beta_1 a)=0$, which yields $\beta_m=m\pi/a=s_m, m\geqslant 1$. The eigenvectors are the same as in the finite-conducting situations (A_1^1,C_1^1) and (A_1^2,C_1^2). However, the amplitudes in the metal domain A_2,B_2,C_2,D_2 are all zero, due to the infinitely large T_2 matrix. Since these two modes are double degenerate, we can reorganize the eigenvectors such that $(A_1,C_1)=(1,0)$ and $(A_1,C_1)=(0,1)$. This we see has returned to the solution for a perfect-conducting grating. For the lowest mode where $\beta_1=0$, the eigenvector is still (A_1^2,C_1^2). However, from Eq. (4.3) E_x has infinite large amplitude. So, if we set the amplitude of E_x to unity, the amplitude of E_y (A_1) and E_z (C_1) are both zero in effect. Therefore, in this case, we also return to the solution of eigenmode in a perfect-conducting grating.

Now we can write down the EM fields inside the grating region using eigenmode expansions. The tangential field components are

$$\begin{aligned}E_x(\mathbf{r})=\sum_m\,&[A_m e^{ik_{z,m1}^+z}X_{m1}^+(x)+B_m e^{ik_{z,m1}^-z}X_{m1}^-(x)\\&+C_m e^{ik_{z,m2}^+z}X_{m2}^+(x)+D_m e^{ik_{z,m2}^-z}X_{m2}^-(x)]e^{ik_y y},\end{aligned} \tag{4.34}$$

$$\begin{aligned}E_y(\mathbf{r})=\sum_m\,&[A_m e^{ik_{z,m1}^+z}Y_{m1}^+(x)+B_m e^{ik_{z,m1}^-z}Y_{m1}^-(x)\\&+C_m e^{ik_{z,m2}^+z}Y_{m2}^+(x)+D_m e^{ik_{z,m2}^-z}Y_{m2}^-(x)]e^{ik_y y},\end{aligned} \tag{4.35}$$

$$\begin{aligned}H_x(\mathbf{r})=\sum_m\,&[A_m e^{ik_{z,m1}^+z}U_{m1}^+(x)+B_m e^{ik_{z,m1}^-z}U_{m1}^-(x)\\&+C_m e^{ik_{z,m2}^+z}U_{m2}^+(x)+D_m e^{ik_{z,m2}^-z}U_{m2}^-(x)]e^{ik_y y},\end{aligned} \tag{4.36}$$

$$\begin{aligned}H_y(\mathbf{r})=\sum_m\,&[A_m e^{ik_{z,m1}^+z}V_{m1}^+(x)+B_m e^{ik_{z,m1}^-z}V_{m1}^-(x)\\&+C_m e^{ik_{z,m2}^+z}V_{m2}^+(x)+D_m e^{ik_{z,m2}^-z}V_{m2}^-(x)]e^{ik_y y}.\end{aligned} \tag{4.37}$$

Here $X_{m1}^+(x)$ is the modal function of the E-field x component connected to mode 1 under the upwards k_z wave vector $k_{z,m1}^+$, see the definition in the square brackets in Eqs. (4.3) and (4.8). Others are similarly defined. A_m,B_m,C_m,D_m are modal coefficients. For the lowest mode $m=0$, since only mode 2 is present, A_m and B_m vanish.

To solve the scattering of a plane EM wave by the 1D metallic lamellar grating, we use the boundary conditions at the two interfaces of $z=h$ and $z=0$. We also use the method of moment similar to that employed in the case of a perfect-conducting grating. We project the E field onto the plane wave basis and obtain

$$C_0 e^{ik^+_{z,02}h} I^{(3)}_{i,0} + D_0 e^{ik^-_{z,02}h} I^{(4)}_{i,0} + \sum_{m\geq 1} [A_m e^{ik^+_{z,m1}h} I^{(1)}_{i,m} + B_m e^{ik^-_{z,m1}h} I^{(2)}_{i,m} + C_m e^{ik^+_{z,m2}h} I^{(3)}_{i,m} + D_m e^{ik^-_{z,m2}h} I^{(4)}_{i,m}] = dE_{xi}(h), \tag{4.38}$$

$$C_0 e^{ik^+_{z,02}h} J^{(3)}_{i,0} + D_0 e^{ik^-_{z,02}h} J^{(4)}_{i,0} + \sum_{m\geq 1} [A_m e^{ik^+_{z,m1}h} J^{(1)}_{i,m} + B_m e^{ik^-_{z,m1}h} J^{(2)}_{i,m} + C_m e^{ik^+_{z,m2}h} J^{(3)}_{i,m} + D_m e^{ik^-_{z,m2}h} J^{(4)}_{i,m}] = dE_{yi}(h), \tag{4.39}$$

$$C_0 I^{(3)}_{i,0} + D_0 I^{(4)}_{i,0} + \sum_{m\geq 1} [A_m I^{(1)}_{i,m} + B_m I^{(2)}_{i,m} + C_m I^{(3)}_{i,m} + D_m I^{(4)}_{i,m}] = dE_{xi}(0), \tag{4.40}$$

$$C_0 J^{(3)}_{i,0} + D_0 J^{(4)}_{i,0} + \sum_{m\geq 1} [A_m J^{(1)}_{i,m} + B_m J^{(2)}_{i,m} + C_m J^{(3)}_{i,m} + D_m J^{(4)}_{i,m}] = dE_{yi}(0). \tag{4.41}$$

Here the moment between a plane wave function and a modal function is defined as

$$I^{(1)}_{i,m} = \int_0^d e^{-ik_{xi}x} X^+_{m1}(x)\,dx, \quad I^{(2)}_{i,m} = \int_0^d e^{-ik_{xi}x} X^-_{m1}(x)\,dx,$$

$$I^{(3)}_{i,m} = \int_0^d e^{-ik_{xi}x} X^+_{m2}(x)\,dx, \quad I^{(4)}_{i,m} = \int_0^d e^{-ik_{xi}x} X^-_{m2}(x)\,dx.$$

$J^{(k)}_{i,m}$, $M^{(k)}_{i,m}$, and $N^{(k)}_{i,m}$ ($k=1,2,3,4$) are obtained by replacing $X(x)$ by $Y(x)$, $U(x)$, and $V(x)$ in the integration, respectively.

The boundary condition for the H-field is matched by projecting the H_x field onto the modal functions of mode 1, while projecting the H_y field onto the modal functions of mode 2. This results in

$$C_0 e^{ik^+_{z,02}h} S^{(3)}_{m,0} + D_0 e^{ik^-_{z,02}h} S^{(4)}_{m,0} + \sum_{m'\geq 1} [A_{m'} e^{ik^+_{z,m'1}h} S^{(1)}_{m,m'} + B_{m'} e^{ik^-_{z,m'1}h} S^{(2)}_{m,m'} + C_{m'} e^{ik^+_{z,m'2}h} S^{(3)}_{m,m'} + D_{m'} e^{ik^-_{z,m'2}h} S^{(4)}_{m,m'}] = \sum_i H_{xi}(h) M^{(1)}_{-i,m}, \tag{4.42}$$

$$m=1,2,\ldots,$$

$$C_0 e^{ik^+_{z,02}h} T^{(3)}_{m,0} + D_0 e^{ik^-_{z,02}h} T^{(4)}_{m,0} + \sum_{m'\geq 1} [A_{m'} e^{ik^+_{z,m'1}h} T^{(1)}_{m,m'} + B_{m'} e^{ik^-_{z,m'1}h} T^{(2)}_{m,m'} + C_{m'} e^{ik^+_{z,m'2}h} T^{(3)}_{m,m'} + D_{m'} e^{ik^-_{z,m'2}h} T^{(4)}_{m,m'}] = \sum_i H_{yi}(h) N^{(3)}_{-i,m}, \tag{4.43}$$

$$m=0,1,2,\ldots,$$

$$C_0 S^{(3)}_{m,0} + D_0 S^{(4)}_{m,0} + \sum_{m'\geq 1} [A_{m'} S^{(1)}_{m,m'} + B_{m'} S^{(2)}_{m,m'} + C_{m'} S^{(3)}_{m,m'} + D_{m'} S^{(4)}_{m,m'}] = \sum_i H_{xi}(0) M^{(1)}_{-i,m}, \tag{4.44}$$

$$m=1,2,\ldots,$$

$$C_0 T^{(3)}_{m,0} + D_0 T^{(4)}_{m,0} + \sum_{m'\geq 1} [A_{m'} T^{(1)}_{m,m'} + B_{m'} T^{(2)}_{m,m'} + C_m T^{(3)}_{m,m'} + D_{m'} T^{(4)}_{m,m'}] = \sum_i H_{yi}(0) N^{(3)}_{-i,m}, \tag{4.45}$$

$m=0,1,2,\ldots$. The moment between two modal functions is defined as

$$S^{(1)}_{m,m'} = \int_0^d U^+_{m1}(x) U^+_{m'1}(x)\,dx,$$

$$S^{(2)}_{m,m'} = \int_0^d U^+_{m1}(x) U^-_{m'1}(x)\,dx,$$

$$S^{(3)}_{m,m'} = \int_0^d U^+_{m1}(x) U^+_{m'2}(x)\,dx,$$

$$S^{(4)}_{m,m'} = \int_0^d U^+_{m1}(x) U^-_{m'2}(x)\,dx,$$

$$T^{(1)}_{m,m'} = \int_0^d V^+_{m2}(x) V^+_{m'1}(x)\,dx,$$

$$T^{(2)}_{m,m'} = \int_0^d V^+_{m2}(x) V^-_{m'1}(x)\,dx,$$

$$T^{(3)}_{m,m'} = \int_0^d V^+_{m2}(x) V^+_{m'2}(x)\,dx,$$

$$T^{(4)}_{m,m'} = \int_0^d V^+_{m2}(x) V^-_{m'2}(x)\,dx.$$

From Eqs. (4.38)–(4.45) we can delete the unknown variables for the modal amplitude, and obtain the following matrix equation that connect the E and H fields in both sides of the grating

$$\begin{pmatrix} E_{xi}(h) \\ E_{yi}(h) \\ E_{xi}(0) \\ E_{yi}(0) \end{pmatrix} = \begin{pmatrix} P_{11} & P_{12} & P_{13} & P_{14} \\ P_{21} & P_{22} & P_{23} & P_{24} \\ P_{31} & P_{32} & P_{33} & P_{34} \\ P_{41} & P_{42} & P_{43} & P_{44} \end{pmatrix} \begin{pmatrix} H_{xi}(h) \\ H_{yi}(h) \\ H_{xi}(0) \\ H_{yi}(0) \end{pmatrix}, \tag{4.46}$$

where $E_{xi}(h)$, etc., implies a column vector with the index "i" ranging between $-N \leqslant i \leqslant N$. This directly leads to the R-matrix formula for the scattering of a single $k_y = k_{yj}$ component of plane wave by one single layer of the 2D layer-by-layer metallic grating

$$\begin{pmatrix} \Omega_{0,j}^{+} \\ \Omega_{1,j}^{+} \end{pmatrix} = \begin{pmatrix} r_{11}^{(j)} & r_{12}^{(j)} \\ r_{21}^{(j)} & r_{22}^{(j)} \end{pmatrix} \begin{pmatrix} \Omega_{0,j}^{-} \\ \Omega_{1,j}^{-} \end{pmatrix}. \tag{4.47}$$

For the whole 2D scattering problem, we directly write down

$$\begin{pmatrix} \Omega_{0}^{+} \\ \Omega_{1}^{+} \end{pmatrix} = \begin{pmatrix} r_{11} & r_{12} \\ r_{21} & r_{22} \end{pmatrix} \begin{pmatrix} \Omega_{0}^{-} \\ \Omega_{1}^{-} \end{pmatrix}, \tag{4.48}$$

where $\Omega_{0,j}^{+}$, Ω_{0}^{+}, etc., have the same definition as in the perfect-conducting case [see Eqs. (3.5) and (2.14)]. Now that we have already derived the R matrix for a single layer of the 2D grating, we can use the R-matrix technique of the transfer-matrix method to solve the scattering problem by a multilayer highly conducting 2D metallic grating slab. This can yield the transmission, reflection, and absorption spectra under an arbitrary plane EM wave incidence. The transmittance T and reflectance R are calculated by means of Eqs. (3.21) and (3.22). The absorptance is calculated according to $A = 1 - T - R$.

In our above solution for a highly conducting grating, we have omitted terms with a factor $e^{i\beta_2(d-a)}$, assuming a small skin depth. To maintain better accuracy, one can include this factor. After some tedious algebra [the detail not shown here, but close to the procedure from Eq. (4.12) to Eq. (4.28)], we find that the eigenvalue β_1 satisfies the following complex transcendent equations

$$\cos(\beta_1 a)\cos[\beta_2(d-a)] - \cos(k_{0x}d) - \frac{1}{2}\sin(\beta_1 a)\sin[\beta_2(d-a)]\left(\frac{\beta_2}{\beta_1} + \frac{\beta_1}{\beta_2}\right) = 0, \tag{4.49}$$

$$\cos(\beta_1 a)\cos[\beta_2(d-a)] - \cos(k_{0x}d) - \frac{1}{2}\sin(\beta_1 a)\sin[\beta_2(d-a)]\left(\frac{\epsilon_2\beta_1}{\epsilon_1\beta_2} + \frac{\epsilon_1\beta_2}{\epsilon_2\beta_1}\right) = 0, \tag{4.50}$$

for modes 1 and 2, respectively. The corresponding eigenvectors are still $(A_1^1, C_1^1) = (1, -k_y/k_z)$ and $(A_1^2, C_1^2) = (k_y/k_z, 1)$. It should be noted that different approaches have been used in earlier literatures[29,30] to solve the scattering problem for a general lamellar grating under conical incidence, leading to the same result of Eqs. (4.49) and (4.50). In Ref. 29, the mathematical problem such as the completeness and orthogonality of the eigenmodes has been addressed in great detail. According to Ref. 29, the eigenmodes of Eqs. (4.29) and (4.30), or Eqs. (4.49) and (4.50) will comprise a complete set of basis for EM fields in our conical scattering problem. It can be found from Eqs. (4.29), (4.30), (4.49), and (4.50) that the eigenvalues β_1 and β_2 have no dependence on the off-plane wave vector k_y. Therefore, the virtual eigenproblem is same for both the in-plane incidence and off-plane conical incidence, a beautiful characteristic for a 1D grating that has been strongly emphasized on in Ref. 29. When $k_y = 0$, $(A_1^1, C_1^1) = (1,0)$, $(A_1^2, C_1^2) = (0,1)$, modes 1 and 2 are exactly the TE and TM modes, respectively. Therefore, Eqs. (4.29) and (4.49) are eigenequation for the TE mode, while Eqs. (4.30) and (4.50) are for the TM mode.

Equations (4.49) and (4.50) are applicable to any value of ϵ_2 in the lamellar grating, either dielectric or metallic. For a highly conducting metallic grating working in the mid-IR regime, Eqs. (4.49) and (4.50) will reduce to Eqs. (4.29) and (4.30), for which fast convergent iteration technique is available in Eqs. (4.31) and (4.32). However, for more general metallic gratings, such as those working in the optical wavelengths, where the skin depth of metal is not too small, one must turn to Eqs. (4.49) and (4.50) for solution. The iteration technique fails completely, other accurate and efficient but much more complicated numerical tools such as the one developed in Ref. 31 can be used to find the eigenvalues. On the other hand, since the dielectric constant for a metal in the optical wavelengths is only modest (in order from 1 to 100), one can use other more flexible numerical schemes such as the Fourier-space coupled-wave method and the real-space transfer-matrix method to solve the scattering problem. The latter two methods seem to be more suitable and efficient for this task.[21,22,32]

V. RESULTS AND DISCUSSIONS

To demonstrate the effectiveness and efficiency of the developed method, we take into account two experiments on the layer-by-layer metallic photonic crystal as examples. The first example we consider is the experiment reported in Ref. 8, where two different structures of layer-by-layer aluminum photonic crystals working in the microwave regime are examined. In one structure, the rectangular aluminum rods are stacked into a fct lattice; in another structure, the rods are stacked into a simple tetragonal (st) lattice, which is similar to the fct lattice, except that rods in the third and fourth layers do not have a $d/2$ shift relative to those in the first and second layers. The measured transmission spectra under normal incidence are shown in Fig. 4(a) (reproduced from Ref. 8) for six-layer samples with a rod-to-rod spacing, rod width and thickness of 7.6, 0.8, and 2.5 mm, respectively. A wide stop band gap and 7–8 dB per layer attenuation are found in both lattices. In addition, there is a significant relative shift of the band gap edge between the fct (22 GHz) and st (20 GHz) lattices. We have performed numerical simulations on these two structures, assuming aluminum a perfect conductor. Good convergence has been reached using only 81 plane waves and 81 modes, and the results are displayed in Fig. 4(b). Excellent agreement with the experimental data can be found: Not only the band edge position and relative shift, but also the attenuation ratio are correctly reproduced. The 2 GHz relative shift suggests that the global lattice structure

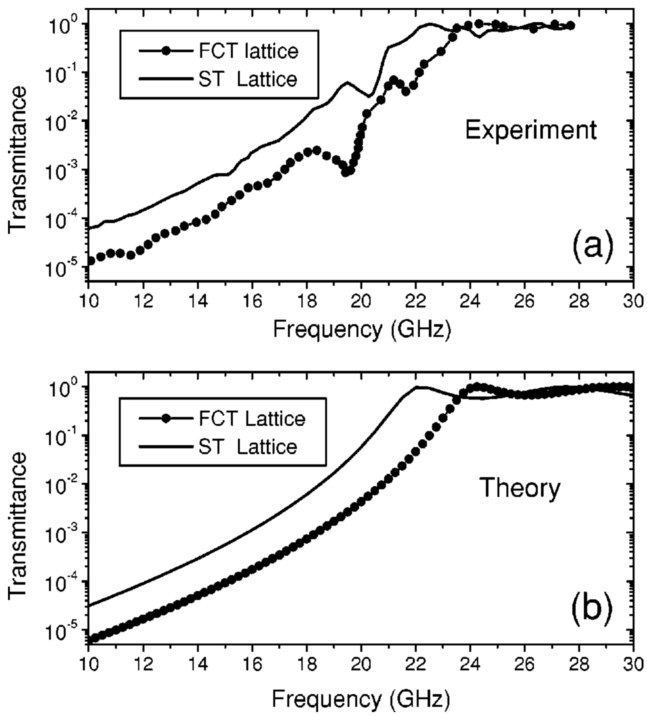

FIG. 4. Transmission spectra for six-layer microwave layer-by-layer aluminum photonic crystals stacked in fct and st lattices. (a) Experimental results, (b) theoretical results. The two crystals each has a rod-to-rod spacing of 7.6 mm, a rod width and thickness of 0.8 and 2.5 mm, respectively.

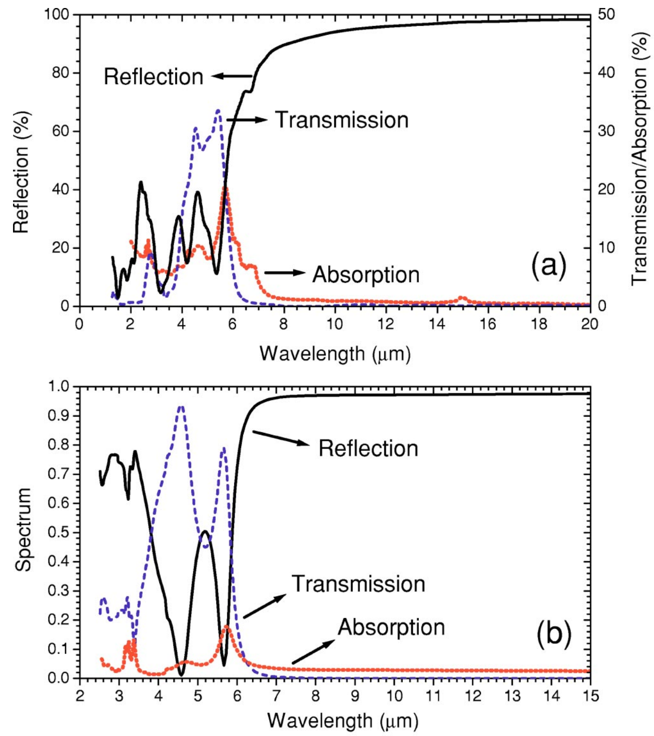

FIG. 5. Transmission, reflection, and absorption spectra for a four-layer mid-IR layer-by-layer tungsten photonic crystal under normal incidence of an unpolarized plane wave. (a) Experimental results, (b) theoretical results. The crystal is stacked by rectangular tungsten rods with a rod-to-rod spacing of 4.2 μm, a rod width and thickness of 1.2 and 1.5 μm, respectively.

(the PBG effect) plays an important role in the formation of this lowest stop band gap.

We now turn to the mid-IR metallic photonic crystal structure[10] made of four-layer rectangular tungsten rods arrayed in a fct lattice. The crystal has a rod-to-rod spacing, rod width and thickness of 4.2, 1.2, and 1.5 μm, respectively. The measured transmission, reflection, and absorption spectra are shown in Fig. 5(a) for an unpolarized plane wave incident along the (001) direction of the crystal. A high reflection and low transmission range appears above $\lambda \sim 6$ μm, which is recognized to be the stop band gap. Below this wavelength, the reflectance exhibits oscillations, and a distinct high-transmission band stands out with two peaks located at about 5.5 and 4.5 μm. Surprisingly, a sharp absorption peak (up to 20.5%) is observed at about 5.7 μm, near the photonic band edge, where the absorption by a bulk tungsten (say, a homogeneous tungsten slab) should be negligible (the reflection coefficient for tungsten at 6 μm is about 98%).

To understand these interesting features, we have done simulations using the analytical modal method for this highly conducting photonic crystal grating structure. The experimental data of the dielectric function of tungsten have been used in the calculations. At $\lambda=6$ μm, tungsten has $\epsilon=-748+205i$, the corresponding skin depth is about 35 nm, two orders of magnitude smaller than the incident wavelength. Good convergence has been achieved also using only 81 plane waves and 81 modes. The results are displayed in Fig. 5(b), where an average over two polarizations of the incident plane wave is taken. A stop band gap extends from about 6 μm to zero frequency. Above that band gap edge, two high transmission bands are observed corresponding to the pass bands of the metallic photonic crystal. The two transmission peaks are located at 4.6 and 5.6 μm, excellently agreeing with the experimental data. Two high reflection bands peaked at around 5 and 3 μm accord well with the oscillation pattern in the experimental reflection spectrum. More impressively, there is indeed a strong absorption peak (with a value 18%) located at 5.7 μm, the same as the experiment. Present in both experiment and theory, this absorption peak should be an intrinsic characteristic of the layer-by-layer metallic photonic crystal structure. As the metal itself shows negligible absorption at 5.7 μm, we ascribe this absorption enhancement to the slow down of wave propagation near the photonic band gap and the high transmission of wave at this wavelength. Both mechanisms increase the flow of wave through the whole metallic structure, and thus enhance the absorption. Indeed, the absorption peak is close to the band edge and the 5.6 μm transmission peak. The other two lower absorption peaks centered at 4.6 and 3.3 μm in the theoretical curve can also be explained by these two mechanisms. Despite the good agreement between experiment and theory regarding the transmission, reflection, and absorption peak positions, there is a quantitative difference in the absolute value. For example, the maximum experimental transmittance and reflectance are much lower than the theoretical values. This quantitative inconsistence can be attributed to the fact that in our calculations, no scattering effects due to disorders and surface roughness of metal rods are considered. Scattering will reduce the transmission and reflection, and increase the absorption. Such a scattering is apparent in the experimental data: The sum of transmittance, reflectance, and absorbance is well below unity.

VI. SUMMARY AND CONCLUSION

In summary, we have developed an analytic modal expansion method in combination with a transfer-matrix technique to examine the reflection, transmission, and absorption spectra of 3D layer-by-layer metallic photonic crystal gratings working in the microwave and infrared wavelengths. In addition, the structural symmetry between different layers of the crystal is fully exploited to connect the transfer matrix for different layers. This has significantly reduced the computation effort on the wave scattering problem. With the aid of this developed electromagnetic approach, fast convergence of numerical result has been obtained and excellent agreement of theoretical results with experimental measurements has been achieved from the microwave to the infrared wavelength regimes. This indicates that the developed electromagnetic method is effective and efficient in handling wave propagation problem for the important class of 3D photonic crystals: layer-by-layer metallic photonic crystals.

ACKNOWLEDGMENTS

Ames Laboratory is operated for the US Department of Energy (DOE) by Iowa State University under Contract No. W-7405-Eng-82. The authors thank Dr. S. Y. Lin for helpful discussions.

[1] E. Yablonovitch, Phys. Rev. Lett. **58**, 2059 (1987).
[2] J. D. Joannopoulos, R. D. Meade, and J. N. Winn, *Photonic Crystals* (Princeton University Press, Princeton, NJ, 1995).
[3] E. R. Brown and O. B. MacMahon, Appl. Phys. Lett. **67**, 2138 (1995).
[4] M. Sigalas, C. T. Chan, K. M. Ho, and C. M. Soukoulis, Phys. Rev. B **52**, 11 744 (1995).
[5] D. F. Sievenpiper, M. E. Sickmiller, and E. Yablonovitch, Phys. Rev. Lett. **76**, 2480 (1996).
[6] S. Fan, P. R. Villeneuve, and J. D. Joannopoulos, Phys. Rev. B **54**, 11 245 (1996).
[7] E. Özbay, B. Temelkuran, M. Sigalas, G. Tuttle, C. M. Soukoulis, and K. M. Ho, Appl. Phys. Lett. **69**, 3797 (1996).
[8] B. Temelkuran, H. Altug, and E. Özbay, IEE Proc.: Optoelectron. **145**, 409 (1998).
[9] W. Y. Zhang, X. Y. Lei, Z. L. Wang, D. G. Zheng, W. Y. Tam, C. T. Chan, and P. Sheng, Phys. Rev. Lett. **84**, 2853 (2000).
[10] J. G. Fleming, S. Y. Lin, I. El-Kady, R. Biswas, and K. M. Ho, Nature (London) **417**, 52 (2002).
[11] K. M. Ho, C. T. Chan, C. M. Soukoulis, R. Biswas, and M. Sigalas, Solid State Commun. **89**, 413 (1994).
[12] S. Y. Lin, J. G. Fleming, D. L. Hetherington, B. K. Smith, R. Biswas, K. M. Ho, M. M. Sigalas, W. Zurbrzycki, S. R. Kurtz, and J. Bur, Nature (London) **394**, 251 (1998).
[13] J. G. Fleming and S. Y. Lin, Opt. Lett. **24**, 49 (1999).
[14] S. Noda, K. Tomoda, N. Yamamoto, and A. Chutinan, Science **289**, 604 (2000).
[15] K. M. Ho, C. T. Chan, and C. M. Soukoulis, Phys. Rev. Lett. **65**, 3152 (1990).
[16] Z. Y. Li, J. Wang, and B. Y. Gu, Phys. Rev. B **58**, 3721 (1998).
[17] N. Stefanou, V. Yannopapas, and A. Modinos, Comput. Phys. Commun. **113**, 49 (1998).
[18] A. Moroz, Phys. Rev. B **51**, 2068 (1995); A. Moroz and C. Sommers, J. Phys.: Condens. Matter **11**, 997 (1999).
[19] M. G. Moharam, E. B. Grann, D. A. Pommet, and T. K. Gaylord, J. Opt. Soc. Am. A **12**, 1068 (1995).
[20] L. Li, J. Opt. Soc. Am. A **13**, 1870 (1996).
[21] L. Li, J. Opt. Soc. Am. A **14**, 2758 (1997).
[22] J. B. Pendry, J. Mod. Opt. **41**, 209 (1994).
[23] P. M. Bell, J. B. Pendry, L. Marin Moreno, and A. J. Ward, Comput. Phys. Commun. **85**, 306 (1995).
[24] J. R. Andrewartha, J. R. Fox, and I. J. Wilson, Opt. Acta **26**, 69 (1979).
[25] L. C. Botten, M. S. Craig, R. C. McPhedran, J. L. Adams, and J. R. Andrewartha, Opt. Acta **28**, 1087 (1981).
[26] L. C. Botten, M. S. Craig, and R. C. McPhedran, Opt. Acta **28**, 1103 (1981).
[27] P. Sheng, R. S. Stepleman, and P. N. Sanda, Phys. Rev. B **26**, 2907 (1982).
[28] L. Li, J. Opt. Soc. Am. A **10**, 2581 (1993).
[29] L. Li, J. Mod. Opt. **40**, 553 (1993).
[30] S.-E. Sandström, G. Tayeb, and R. Petit, J. Electromagn. Waves Appl. **7**, 631 (1993).
[31] G. Tayeb and R. Petit, Opt. Acta **31**, 1361 (1984).
[32] I. El-Kady, M. M. Sigalas, R. Biswas, K. M. Ho, and C. M. Soukoulis, Phys. Rev. B **62**, 15 299 (2000).